MAREES TERRESTRES

BULLETIN D'INFORMATIONS

106

10 JANVIER 1990

Association Internationale de Geodesie

Commission Permanente des Marees Terrestres

Editeur Prof. Paul MELCHIOR

Observatoire royal de Belgique

Avenue Circulaire 3

1180 Bruxelles

BIM 106

15 December 1989

The effect of humidity variations on long-term tidal gravity recordings.

R. Bastien and A.K. Goodacre
*Geophysics Division, Geological Survey of Canada.**

Large annual signals of the order of 200-500 μGal in amplitude are a common feature of continuous long-term gravity tide recordings. It has been previously suggested that these oscillations are the result of annual variations in either ambient temperature or humidity. Since March 1985, the gravity meter LaCoste & Romberg ET-12 has been continuously recording at the Geophysical Laboratory, Geological Survey of Canada, Ottawa. By operating in a controlled environment it has been possible to investigate the effect of humidity on the recording gravity meter. Results demonstrate clearly that the large annual signal in the output of ET-12 is caused by humidity.

De grandes oscillations annuelles de l'ordre de 200 à 500 μGal d'amplitude sont généralement observées sur les enregistrements continus de longue durée de la marée terrestre. On avait précédemment suggéré que ces oscillations pouvaient dépendre des variations annuelles de la température ou de l'humidité ambiante. Depuis mars 1985, le gravimètre ET-12 de LaCoste et Romberg enregistre continuellement au Laboratoire de Géophysique de la Commission Géologique du Canada à Ottawa. Son fonctionnement dans un environnement contrôlé a permis une analyse de l'effet de l'humidité sur l'enregistrement du gravimètre. Les résultats démontrent clairement qu'une variation importante du signal du ET-12 est causée par l'humidité.

Drift history of ET-12

The Earth-tide meter ET-12 was purchased from Lacoste & Romberg in 1967 to gather data for research into Earth tides and to support microgravity field surveys. An Earth tide meter, if not moved, drifts normally with time because of the aging of the spring and ligatures. But in fact we have observed some oscillations due to environmental effects such as atmospheric pressure, tilt of the floor or some unknown sources. A normal secular drift for this type of meter would be about 1 mGal per year.

In 1974, seven years after we purchased the meter, the drift rate began to change. At that point, something was not working normally. But for various reasons, the meter was not used on a regular basis until 1985.

---

* *1 Observatory Cr. Ottawa, Ontario, Can. K1A 0Y3*

The annual oscillation of ET-12 output.

In 1985, we started again to record Earth tides on a continuous basis. At the beginning, the data were used to study outdoor environmental effects such as rainfall on ET-12 gravity recordings. The meter was later used also to support the development of the absolute gravity meter in Ottawa. We have now four years of continuous hourly data that have been recorded in both normal and controlled environments. After two years, we could clearly identify an annual signal superimposed on a linear trend (see Figure 1).

Since 1978, Lacoste & Romberg gravity meter G-7 was used to display the Earth tide to the general public. On a quarterly basis, the meter was reset in order to keep the pen on the paper of the chart recorder. A plot of the resets over a period of seven years showed that an annual signal of about 1.3 mGal peak-to-trough was present (C. Gagnon, pers. comm.). At about the same time, we noted that a signal with the same period was also present on the chart recordings from ET-12, but with a smaller amplitude of about 0.5 mGal peak-to-trough. The maximum and minimum of this wave occured in October and April, respectively.

A simple model of the form $Y = a + b*t + c*\sin(2\pi t/T) + d*\cos(2\pi t/T)$ was fitted to the ET-12 data set, and gave a drift $b = -620$ μGal/year, a long-term period $T = 343$ days with an amplitude $A = \sqrt{c^2 + d^2} = 450$ μGal peak-to-trough.

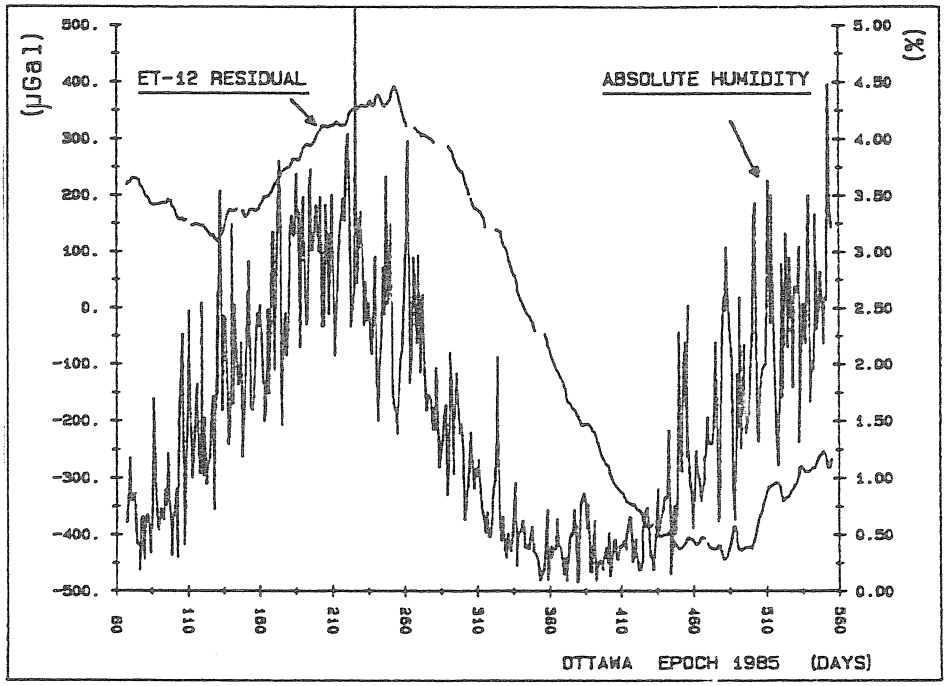

Figure 1. Plot of ET-12 output (smooth line) and outside humidity.

Some other results

Gerstenecker and Schüller (1983) obtained a similar kind of result in Zurich with ET-16. At that time, the annual oscillation of 200 μGal peak-to-trough was correlated to the outdoor temperature and assumed to be caused by it. Doing a cross-correlation between ET-16 and outdoor temperature they found that the temperature was leading the residual drift by 30 days.

Asch et al. (1985) showed large annual waves recorded by two gravity meters: Askania GS-15 and Lacoste & Romberg ET-18. The amplitude of the wave from GS-15 was nearly 1 mGal and the amplitude of the ET-18 about 600 μGal peak-to-trough. They concluded that the yearly period was correlated with *the air humidity in the installation room.*

Choice of humidity as the responsible factor

If we compare the outdoor temperature to the absolute humidity for the same period of time, we realise that they are strongly correlated with both factors having an annual oscillation. A cross-correlation confirms a good correlation between humidity and temperature with no phase lag, the maximum correlation being for a phase difference of zero. In fact, since the temperature inside the room was controlled all year but not the humidity, we thought that humidity might be the better explanation.

Humidity was not recorded inside the room in the period 1985-86 but we do have records of the outside humidity. We can assume that the average absolute outside humidity is nearly the same as inside since humidity is not controlled. In Figure 1, there is a representation of the ET-12 residual with the absolute humidity for a duration of 500 days. The graph shows that humidity is leading ET-12 output by one or two months. A cross-correlation between ET-12 and humidity confirms that humidity is effectively leading the output of ET-12 by some 60 days (see Figure 2).

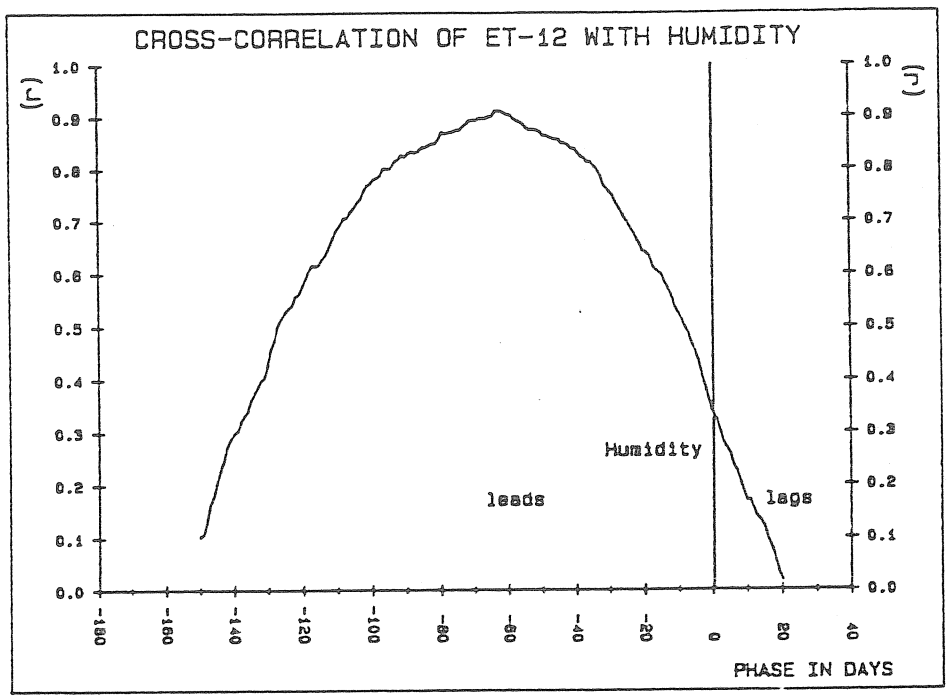

Figure 2. Humidity leads ET-12 by 60 days. Cross-correlation applied on data shown on Figure 1.

Installation in a controlled environment

Suspecting that humidity might be the cause of the problem, we installed a plexiglass box over the Earth tide meter in order to control humidity inside the box. The box consists of a frame that is glued to the cement floor. The frame is arranged to receive the box in a 3 inch deep slot with a seal in the bottom of the slot. The temperature was already controlled in the room. The experiment started with a low humidity level using about one gallon of Silica Gel desiccant to keep

the air as dry as possible inside the box. The pressure was able to equilibrate inside and outside the box via a tube that was passing through a small container of desiccant. Relative humidity and temperature were recorded inside the box with an interval of one hour but only after application of a Kalman filter using a one-minute sampling interval.

Results with a low-humidity environment

After one year of low-humidity control, the sinusoidal character of the gravity meter output disappeared, thus confirming that humidity was in fact the cause of the annual signal since only that variable was changed. A low-humidity control corresponds in this case to keeping the relative humidity to 10% at 22 degree C. Absolute humidity was calculated to be between 0.2% and 0.5%. Figure 3 shows that the output of ET-12 was still going down in October despite the fact that at this period of the year, the signal was normally at its maximum.

An exponential model of the form $Y = a + b*t + c*e^{(-t/T)}$ was fitted to the trend. The model includes a constant, a linear time-dependent term and an exponential time term. The different coefficients were determined using an iterative convergence technique combined with a least-squares adjustment. This model gives the long-term drift as -640 μGal/year which is close to the normal long-term drift of -620 μGal/year found earlier. The time constant T of the exponential term is about 100 days.

Results with a high-humidity environment

In October 1987, the situation was reversed. We replaced the desiccant by water. The relative humidity in the box climbed to nearly 100% in a few days. In absolute terms, the humidity was kept between 2% and 3%. It is preferable to speak in terms of absolute humidity because it is independent of temperature. In fact, absolute humidity is the ratio between the water vapour pressure and the total pressure.

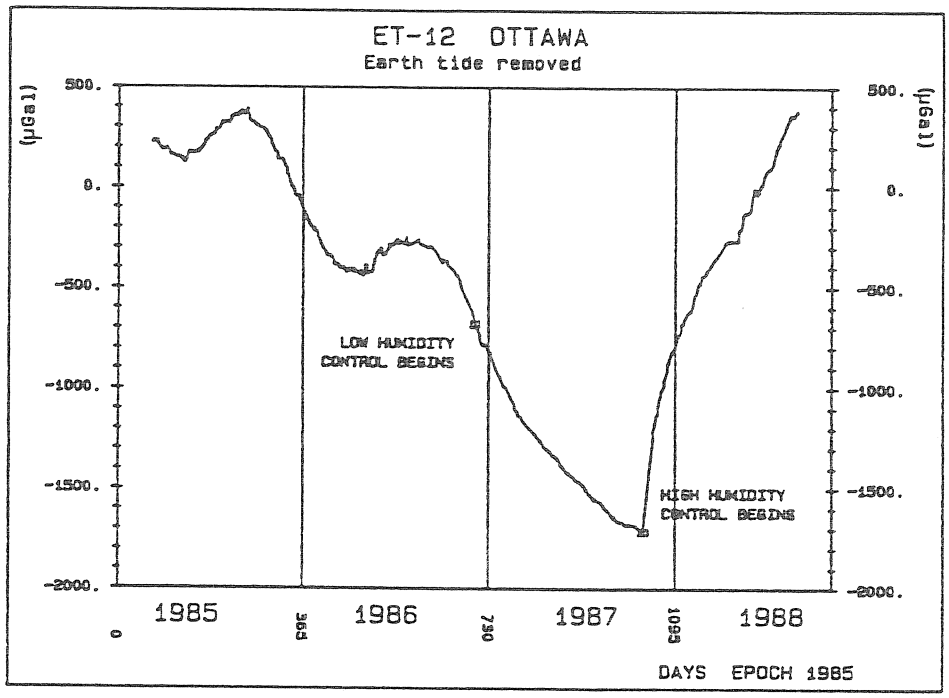

Figure 3. Drift history of ET-12 since 1985, in normal and controlled environments.

After another year of observation in a high-humidity environment, the ET-12 output was giving the opposite result (see Figure 3). This second experiment demonstrates how humidity is such an important factor. In one year, the reading of the meter went up by some 2 mGal, an amount that would normally take 3 years to lose.

Again, an exponential model was fitted to the positive trend. This model is the same as for the negative trend and was computed using the same method. The best fit gave a long-term positive drift of 1.7 mGal/year with a time constant of only 22 days as opposed to the 100 days that we obtained during low-humidity control. It seems that the time response with a low-humidity step is longer than the time response with a high-humidity step. This means that a cross-correlation between cyclic variations in humidity and ET-12 should show that humidity leads by an amount of time lying in the interval of 20 to 100 days.

Possible explanations

The observed humidity effect might have been caused by the electronics inside the enclosure of ET-12. In particular, it was thought possible that the resistivity of the printed circuit was modified due to a surface deposit of water. So all the printed circuits of the meter were dried and sprayed with a silicone resin coating. This treatment seems to have had no effect at all since ET-12 continued to display the same positive drift.

An alternative possibility is that the meter is not properly sealed and that humidity simply gets into the inner enclosure. The problem could presumably be solved simply by replacing the seals; Lacoste & Romberg suggests once every five years. The possible mechanical or structural effects are not clearly explained. Hygroscopic materials may be the best explanation because their weight will vary with the amount of water they absorb. Adsorbtion is another possibility, since any material accepts a certain layer of water on its surface in a humid environment. Oxidation may be another explanation although, as far as we know, it has not been observed. In every case, seals should, as recommended by the manufacturer, be replaced on a regular basis. We can conclude that the direct cause of large annual signals in our Earth tide meters is humidity.

Acknowledgements

Thanks to Carey Gagnon for his advice and support. Contribution of the Geological Survey of Canada No. 43188.

Asch, G., Elster, C., Jentzsch, G., and Plag, H.-P., 1985. On the estimation of significant periodic and aperiodic gravity variations in the time series of neighbouring stations - Part II: Non-tidal signals. Proceedings of the Tenth International Symposium on Earth Tides, pp. 251-262.

Bower, D.R., Lambert A. and O'Brien J. 1976. Tidal gravity measurements at Ottawa and Alert, 1967-1974. Geodynamics Series Bulletin No. 67. Ottawa, Canada. 65 pages.

Gerstenecker, C. and Schüller, K., 1983. Nonlinearity and drift behavior of a LaCoste-Romberg Earth-tide Gravimeter, Proceedings of the Ninth International Symposium on Earth Tides, pp. 261-270.

DETERMINATION OF SOME PARTICULAR WAVES IN THE EARTH TIDE DATA

C. De Toro*, A.P. Venedikov**, R. Vieira*

* Instituto de Astronomia y Geodesia, Madrid

** Geophysical Institute, Sofia

1. Introduction.

Recently Melchior & Ducarme (1986) and Melchior, Crossley, Dehant & Ducarme (1987) (hereinafter MA) have detected, in the observations made by the superconducting gravimeter in Brussels, some new particular waves (hereinafter SW). Their period range is between 13.166 and 17.126, a most significant wave being observed at 13h 924.

Evidently SW are of non-tidal origin. In the spectrum they are situated between the D and SD bands, considerably closer to SD.

Briefly the method for the determination of SW used by MA consists in the following. First the signal preliminary determined is subtracted. Then the residual curve thus obtained is submitted to power spectrum analysis.

Here we shall demonstrate another way to study SW which may be used in addition to the research done by MA. We shall present a few preliminary but more or less encouraging results.

We have an information about the periods (frequencies) of SW theoretically and/or experimentally (MA) determined. Then it becomes possible, even recomendable, to use the Method of the least squares to estimate the elements of SW. The main advantages of this method are (i) we can create and use a clear and flexible mathematical model (or models) and (ii) the results are accompanied by well defined estimates of their precision.

The physical sense of SW is not the object of our paper. We can only refer to the papers of MA, Gunn & Aldridge (1987), Aldridge & Lumb (1988) where one may find an interpretation and a corresponding bibliography. We shall simply note that SW have an extremely low power - amplitude of the order of a few nanogals (10^{-12} of the gravity) - and that they may have variable and unstable amplitudes, phases and frequencies.

2. The analysis model.

The model of the useful tidal signal in the method of analysis (Venedikov, 1966, 1978) is

$$L(t) = \sum_{j=1}^{m} \xi_j \cdot \sum_{i=a_j}^{b_j} H_i \cos (P_i + w_i t)$$

$$+ \eta_j \cdot \sum_{i=a_j}^{b_j} H_i \sin (P_i + w_i t) \qquad (1)$$

where

$L(t)$: tidal signal at time t,

i : index or sequential number of a given tide,

H_i : theoretical (undeformable Earth) amplitude,

P_i : theoretical phase for an initial epoch for which t = 0,

w_i : angular velocity,

a_j, b_j : the tides with indices

$$a_j \leq i \leq b_j \qquad (2)$$

shape a tidal group j (j = 1, 2, ...m); it is supposed that all of them have one and the same tidal parameter δ_j and $\varkappa_j$, and

$$\xi_j = \delta_j \cos \varkappa_j, \qquad \eta_j = -\delta_j \sin \varkappa_j \quad . \qquad (3)$$

The quantities (3) are the unknowns which are determined by the analysis. From them we obtain δ_j and $\varkappa_j$.

Let us suppose that the tidal record incorporates an additional wave of type SW whose angular velocity is w. Analytically this can be represented by the addition to the right side of the expression (1) of a term like

$$L(t) = \xi . H \cos (P + wt) + \eta . H \sin (P + wt) \quad . \qquad (4)$$

This term is composed in such a way in order to be similar to the representation of the tidal waves in (1). Namely H and P are included as theoretical amplitude and phase but they can be choosen absolutely arbitrary. The quantities ξ and η are unknowns about which we have in mind expressions similar to (3). If we obtain ξ and η through a processing of the data, then the observed amplitude h of the wave SW will be calculated after

$$\delta^2 = \xi^2 + \eta^2 \qquad \text{and} \qquad h = \delta \cdot H \qquad . \qquad (5)$$

In MA the periods are given, naturally, with a limited precision, for example 13.924. Evidently one may expect that the last digit is not certain. The uncertainty arises if we suppose that the waves SW change with time. That is why we have made the following numerical speculation.

The single wave (4) is replaced by the sum of 5 waves with very close periods/angular velocities. If T is a given period, these 5 waves have the periods T - 0.0010, T - 0.0005, T, T + 0.0005 and T + 0.0010.

In the computer's program SV there are 504 tides from the Cartwright-Tayler-Edden development plus 3 "meteorological" waves (see Table II). All these waves are enumerated by the index i = 1, 2,..507. Thus the five waves have the indices i = 508,.512. The sum through which the representation (4) is replaced looks like

$$L(t) = \xi \sum_{i=508}^{512} H \cos (P + w_i t) + \eta \sum_{i=508}^{512} H \sin (P + w_i t) \qquad (6)$$

where the arbitrary H and P remain constants for all 5 waves, while w_i are slightly different.

For the period T = 13.924 we have chosen

Table I

i	periods h	w_i o
508	13.9230	25.8565
509	13.9235	25.8556
510	13.9240	25.8546
511	13.9245	25.8537
512	13.9250	25.8528

3. Filters for the determination of SW.

The first stage of the analysis consists in the filtration of independent intervals (intervals without overlapping) from the record which is processed. The length of the intervals most often used is 48 hours but the program SV allows its arbitrary choice, for example 36 hours. In the present study for the determination of SW we have chosen two lengths : 36 and 42 hours. The first one was choosen as we have used it frequently for the determination of the usual D and SD tides, and the second one - as it is approximately multiple (3 times) of the period 13.924.

The filters were constructed through consecutive orthogonalization (Venedikov, 1978). The tables II represent the response (columns SW1) of the filters used. The first of the columns SW1 is for the even filter, the second one - for the odd filter. Only the most important components are included in the tables.

The filters eliminate an arbitrary linear drift independently for each one of the filtered intervals. Their response is just 1.00000 for the component i = 508, i.e. for the first of the 5 waves SW. The D tides are reduced through the perfect elimination of both O1 and S1. However, as the precision for the determination of SW must be a very high one, generally the reduction of D is not satisfactory (Q1, K1). This is taken into account in the analysis.

SW are very close to SD and it is not possible to be separated from them within intervals of such a length. Something more, the response of the filters for SD is higher than 1.00000. This is because SW are between D and SD. If we conceive SW, D and SD as n-dimensional vectors (n = 36 or 42) D and SD are approximately orthogonal and SW lays approximately in the hyperplane (D, SD), between D and SD. The orthogonalization of SW to the D components O1 and S1, through which we obtain filters eliminating O1 and S1, turns SW closer to SD than to the initial position of SW.

4. Some results.

We have processed the series of data obtained by the superconducting gravimeter in Brussels. The data were kindly given at our disposal by prof. Melchior.

They cover a 5.6 years interval : 21.04.1982 - 26.11.1987, a little bit larger than the series used by MA.

Table III represents an output from the program SV for SW with a mean period T = 13.924 (see Table I). It can be seen which tidal groups are included in the computation, i.e. how is composed the model (1).

At first there is one group indicated by K1 which comprises all 205 D tides. It appeared to be necessary to include this group in the model because the separation of SW from D, as it was stated in the previous paragraph, is not a perfect one. This is proved by the fact that the δ factor obtained for this group is a significant one (1.245 ± 0.098). At the same time it is not necessary to use a more detailed separation because D as a whole is strongly suppressed by the filters.

Then there are 13 SD groups - the most detailed separation which is used by the tidal analysis. One can see that we have obtained a very good determination of these tides. After that there is a single group M3 composed by all TD waves. The filters were not designed to eliminate TD.

At the end there is the group of five SW waves (Table I). The digits printed as the argument number of Doodson are of no meanings. Here one can notice that the intermediately value δ = 0.31 is just 100 times the observed amplitude h = 0.0031 μgal = 3.1 nanogal. This is because the arbitrary value of the "theore- tical" amplitude H in (4) and (6) was choosen H = 100.

The extremely high precision of near 1 nanogal is due to the accumulation in the model (6) of 5 waves with very close periods (Table 1). It can be accepted as realistic only if the spectrum is a continuous one over the band defined by the five waves (discussion at the time of the meeting of the Working group on high precision tidal data processing and particular remark by prof. Jentzsch). In fact if we want to attribute the result to a single wave, i.e. a single line in the spectrum we have to multiply both the amplitude and its R.M.S. (mean square error) by a factor near 5. For differences between the 5 frequencies as in Table I the factor is 4.8.

In table IV the amplitudes with their R.M.S. (after a multiplication by 4.8) for several periods are given. These are some of the periods obtained by MA. An exception is the first period in the Table IV. It has been chosen as the closest period which can be separated from 13.924 within a record of 5.6 years. It is an important fact that there is not a significant amplitude at this period.

If we use the Student's criterea the amplitude is a significant one only at 13.924. Thus we have only a partly confirmation of the results obtained by MA.

Nevertheless we are more inclined to consider this as encouraging. Our results are to be considered as preliminary ones and they were obtained mainly in order to develop the technology for this way of processing. We realize that there is still room for perfectioning the computation : (i) modification of the program in order to make easier and more operational the work when new particular waves are searched, (ii) better and more motivated choice of the filters including their lengths and eliminated components, (iii) perfectioning of the model, (iv) separation of the whole interval of the data on shorter intervals delimited by strong earthquakes as in MA, (v) introduction of a new tide-potential development,(vi) consideration of the air-pressure influence, (vii) experimentation on other long series of data etc.

We express our thanks to prof. P. Melchior for initiating our research on this interesting and important delicate problem as well as for giving at our disposal the high precision data from the superconducting gravimeter in Brussels.

FILTERS LENGTH 33 NR 102,501,202,

Table II.A

i	waves	w_i^o	SWI	SWI
0	056 554 SA	0.0411	J.000035	0.000000
13	057 555 SSA	0.0821	J.000020	0.000000
16	058 554 STA	0.1232	J.000044	C.000000
32	065 455 MA	0.5444	J.000863	C.000014
50	073 555 MSF	1.0159	J.002975	C.000091
64	075 555 MF	1.0780	J.003469	C.000114
83	083 655 MSTM	1.5696	J.006977	C.000328
95	085 455 MTM	1.8424	J.007617	0.000375
111	093 555 MSSM	2.1139	J.012333	C.000783
122	0*3 455 SK3	2.6583	J.018872	0.001506
129	107 755 1S7	11.8384	J.023233	0.010434
133	115 855 1K5	12.3099	J.020151	C.007715
137	117 655 SISS	12.3328	J.018961	C.007359
140	119 455 1K9	12.4556	J.017775	C.006944
148	125 755 2S1	12.8543	J.011604	C.004717
155	127 555 SIS1	12.9271	J.010628	C.004325
160	129 355 129	13.0000	J.009621	0.003940
166	134 656 134	13.3576	J.005150	0.002178
174	135 645	13.3965	J.004729	C.002002
175	135 655 Q1	13.3987	J.004704	0.001992
182	136 654 136	13.4397	J.004252	C.001811
185	137 455 KQ1	13.4715	J.003928	C.001674
190	138 454 138	13.5126	J.003509	0.001500
195	143 755 143	13.8702	J.000473	0.000208
197	144 556 144	13.9020	J.000260	0.000115
201	145 545	13.9408	J.000014	C.000006
202	145 555 Q1	13.9430	J.000000	0.000000
210	146 554 146	13.9841	-J.000243	-0.000108
214	147 555 TAJ1	14.0252	-J.000469	-0.000209
221	153 655 153	14.4146	-J.001695	-0.000779
226	155 455	14.4374	-J.001728	-0.000799
231	155 655 NQ1	14.4967	-J.001727	-0.000799
237	157 455 CMIL	14.5695	-J.001686	-0.000784
243	162 556 P11	14.9179	-J.000520	-0.000249
246	163 555 P1	14.9589	-J.000272	-0.000131
252	164 556 S1	15.0000	J.000000	0.000000
259	165 545	15.0389	J.000280	0.000135
260	165 555 K1	15.0411	J.000297	0.000143
261	165 565	15.0433	J.000313	0.000151
265	166 554 P511	15.0821	J.000618	0.000299
270	167 555 PM11	15.1232	J.000965	0.000469
278	173 655 TETA	15.5126	J.005553	C.002777
283	175 455 J1	15.5534	J.006683	0.003361
300	183 555 SQ1	16.0370	J.016210	0.008441
309	185 555 QQ1	16.1391	J.018277	C.009574
310	185 565	16.1413	J.018334	C.009606
316	193 455 193	16.6013	J.032293	C.017492
325	195 455 NQ1	16.6335	J.035219	C.019190
328	1*3 555 1K3	17.1550	J.054604	C.030797
334	209 655 209	26.4079	1.051932	1.092043
337	217 755 217	26.8795	1.088793	1.168678
339	219 555 219	26.9523	1.095040	1.180279
343	225 655 JN2	27.3510	1.120747	1.242341
347	227 655 EPS2	27.4253	1.124877	1.253392
352	229 455 229	27.4307	1.128826	1.264345
360	235 755 2N2	27.8754	1.147151	1.322355
361	236 556 235	27.9271	1.143367	1.326830

FILTERS LENGTH 30 NR 102,501,202,

Table II.A (continuation)

i	waves	w_i	SW1	SW1
		o		
367	237 555 MJ2	27.9682	1.149884	1.332575
370	238 554 233	28.0093	1.151339	1.338280
371	239 355 239	28.0411	1.152423	1.342667
377	244 650 244	28.3987	1.162011	1.390239
385	245 655 J2	28.4397	1.162802	1.395480
390	246 654 246	28.4803	1.163523	1.400674
392	247 455 MJ2	28.5126	1.164045	1.404661
397	248 454 248	28.5536	1.164656	1.409768
402	253 755 253	28.9113	1.167193	1.452069
404	254 556 254	28.9430	1.167175	1.455632
409	255 545	28.9819	1.167098	1.459943
410	255 555 M2	28.9841	1.167092	1.460187
417	256 554 256	29.0252	1.166942	1.464685
420	257 553 257	29.0662	1.166725	1.469127
426	263 655 LAMB	29.4556	1.161312	1.508300
430	265 455 L2	29.5285	1.159621	1.515016
438	267 455 267	29.6106	1.157454	1.522345
441	271 557 271	29.9179	1.145952	1.547419
442	272 556 T2	29.9589	1.145259	1.550483
444	273 555 S2	30.0000	1.143493	1.553477
447	274 554 274	30.0411	1.141669	1.556401
453	275 555 K2	30.0821	1.139772	1.559255
454	275 565	30.0843	1.139659	1.559406
463	283 655 283	30.5537	1.113158	1.586815
467	285 455 ETA2	30.6205	1.108259	1.590194
475	293 555 293	31.0980	1.071561	1.606119
481	295 555 2K2	31.1302	1.064299	1.607815
486	2*5 455 2A5	31.7245	1.009885	1.610682
488	327 655 327	41.9159	-0.424439	-0.317834
489	335 755 335	42.3874	-0.432930	-0.405929
492	345 655 345	42.9318	-0.432216	-0.495237
496	355 555 M3	43.4762	-0.420705	-0.570037
498	365 455 365	44.0205	-0.399108	-0.629327
502	375 555 375	44.5742	-0.367733	-0.673008
505	382 555 S3	45.0000	-0.337870	-0.694948
506	455 555 M4	57.9682	0.064187	0.482259
507	491 555 S4	60.0000	-0.095641	0.313101
508	111 111 SM1	25.8505	1.000000	1.000000
509	111 111 SM2	25.8556	0.999906	0.999844
510	111 111 SM3	25.8540	0.999812	0.999687
511	111 111 SM4	25.8557	0.999718	0.999531
512	111 111 SM5	25.8528	0.999624	0.999375

FILTERS LENGTH 42 NR 102,501,202,

Table II.B

i	waves			w_i	Swl	Swl
				o		
9	050	554	SA	0.0411	0.000011	0.000000
13	057	555	SSA	0.0521	0.000042	0.000000
16	063	554	STA	0.1232	0.000095	0.000000
32	065	455	MM	0.5444	0.001847	0.000030
50	073	555	MSF	1.0159	0.006363	0.000190
64	075	555	MF	1.0980	0.007422	0.000240
83	083	055	MSTM	1.5696	0.014910	0.000688
93	085	455	MTM	1.6424	0.016274	0.000786
111	093	555	MSSM	2.1159	0.026319	0.001637
122	095	455	SXM	2.6583	0.040164	0.003144
129	107	755	1QT	11.8384	0.053210	0.019295
133	115	855	115	12.3099	0.037583	0.014224
137	117	055	SIGQ	12.3828	0.033237	0.013440
140	119	455	119	12.4556	0.033025	0.012660
148	125	755	2QT	12.8543	0.021460	0.008517
155	127	555	SIGT	12.9271	0.019518	0.007795
160	129	355	129	13.0000	0.017637	0.007088
166	134	056	134	13.3576	0.009373	0.003882
174	135	045		13.3965	0.008581	0.003566
175	135	055	QT	13.3987	0.008537	0.003548
182	136	054	136	13.4397	0.007725	0.003222
185	137	455	RO1	13.4715	0.007115	0.002975
190	138	454	138	13.5126	0.006346	0.002664
195	143	755	143	13.8702	0.000847	0.000366
197	144	556	144	13.9020	0.000466	0.000202
201	145	545		13.9408	0.000024	0.000011
202	145	555	O1	13.9430	0.000000	0.000000
210	146	554	146	13.9341	-0.000434	-0.000189
214	147	555	TAO1	14.0252	-0.000837	-0.000366
221	153	655	153	14.4146	-0.002991	-0.001350
226	155	455		14.4374	-0.003043	-0.001381
231	155	655	NO1	14.4907	-0.003041	-0.001381
237	157	455	CHI1	14.5095	-0.002962	-0.001353
243	162	556	PI1	14.9179	-0.000904	-0.000425
248	163	555	PI	14.9589	-0.000473	-0.000223
252	164	556	S1	15.0000	0.000000	0.000000
259	165	545		15.0389	0.000435	0.000230
260	165	555	K1	15.0411	0.000514	0.000244
261	165	565		15.0433	0.000543	0.000257
265	166	554	PSI1	15.0821	0.001070	0.000509
270	167	555	PHI1	15.1232	0.001668	0.000795
276	173	655	TETA	15.5126	0.009831	0.004657
283	175	455	J1	15.5534	0.011384	0.005622
300	183	555	SO1	16.0570	0.027194	0.013909
309	185	555	OO1	16.1391	0.030578	0.015735
310	185	565		16.1413	0.030671	0.015785
316	193	455	193	16.6013	0.053135	0.028304
325	195	455	NU1	16.6835	0.057839	0.030963
328	1*3	555	1X3	17.1550	0.083274	0.048876
334	209	655	2N1	26.4079	1.003413	1.045122
337	217	755	2T1	26.8795	0.995571	1.074889
339	219	555	2K1	26.9523	0.993471	1.078706
343	225	655	0N2	27.3510	0.977796	1.095681
349	227	655	EPS2	27.4238	0.974173	1.098048
352	229	455	229	27.4967	0.970313	1.100183
356	235	755	2N2	27.8954	0.945177	1.107665
361	235	556	235	27.9271	0.942832	1.107950

FILTERS LENGTH +2 NR 102,501,202,

Table II.B (continuation)

i	waves			w_i	Sw1	Sw1
				°		
367	237	555	MJ2	27.9582	0.939855	1.108250
370	238	554	238	28.0093	0.936758	1.108472
371	239	555	239	28.0411	0.934313	1.108591
377	244	655	244	28.3967	0.903987	1.106665
385	245	655	N2	28.4397	0.900179	1.106058
390	246	654	246	28.4808	0.896307	1.105371
392	247	455	MJ2	28.5126	0.893254	1.104784
397	248	454	248	28.5556	0.889277	1.103955
402	253	755	253	28.9113	0.851906	1.093333
404	254	556	254	28.9430	0.848361	1.092093
409	255	545		28.9819	0.843980	1.090512
410	255	555	M2	28.9841	0.843729	1.090420
417	256	554	256	29.0252	0.839039	1.088666
420	257	555	257	29.0662	0.834290	1.086831
426	263	655	LAMB	29.4556	0.788515	1.065445
430	265	455	L2	29.5285	0.777049	1.060647
438	267	455	267	29.6106	0.766139	1.054938
441	271	557	271	29.9179	0.723892	1.030800
442	272	556	T2	29.9589	0.718059	1.027245
444	273	555	S2	30.0000	0.712165	1.023613
447	274	554	274	30.0411	0.706239	1.019905
453	275	555	K2	30.0821	0.700271	1.016120
454	275	565		30.0843	0.699949	1.015915
463	283	655	283	30.5537	0.629030	0.967332
467	285	455	ETA2	30.6265	0.617700	0.958940
475	293	555	293	31.0980	0.541960	0.899398
481	295	555	2K2	31.1802	0.528467	0.888137
486	2*5	455	2N5	31.7245	0.437537	0.807377
488	327	655	327	41.9159	-0.035249	-0.333671
489	335	755	335	42.3874	-0.049826	-0.298592
492	345	655	345	42.9318	-0.039289	-0.250491
496	355	555	M3	43.4702	0.029462	-0.196064
498	365	455	365	44.0205	0.066090	-0.137344
502	375	555	375	44.5742	0.099525	-0.075385
505	382	555	S3	45.0000	0.117756	-0.027578
506	455	555	M4	57.9682	-0.034708	-0.210839
507	491	555	S4	60.0000	-0.006443	-0.183146
508	111	111	SM1	25.8505	1.000000	1.000000
509	111	111	SM2	25.8556	0.999983	0.999915
510	111	111	SM3	25.8546	0.999966	0.999831
511	111	111	SM4	25.8537	0.999949	0.999746
512	111	111	SM5	25.8528	0.999932	0.999661

STATION BRUSSELS VERTICAL COMPONENT BELGIUM **Table III**
GRAVIMETER SUPERCONDUCTIVE, OBSERVATOIRE ROYAL DE BELGIQUE
50 48 0 N 4 22 0 E H 101M
P.MELCHIOR

LEAST SQUARE ANALYSIS/VENEDIKOV/74,PROG.SV.-ICET-LUCARME,MELCHIOR,VENEDIKOV
FILTERS ON 30 HRS,NR 102,301,202, ELIM.POWERS SM 1
COMPONENTS S1 O1 SM1 S2 N2
POTENTIAL CARTWRIGHT-TAYLER-EDDEN / COMPLETE DEVELOPMENT
COMPONENTS ORIENTATED TOWARDS THE ELLIPSOID (SKALSKY)
COMPUTER CENTRE UNIVERSITY COMPLUTENCE, MADRID
COMPUTER IBM 4381 PROCESSED ON 15.09.88

NORMALIZATION FACTOR 0.1000
INERTIAL CORRECTIONS INTRODUCED

TIME INTERVAL 5.0 YEARS 2041.0 DAYS 48168 READINGS 3 BLOCKS NO WEIGHTS
GAPS 820421/820525 820802/861014 861115/871126

WAVE GROUP ARGUMENT	N	WAVE	ESTIMATED AMPL.	R.M.S.	AMPLIT. FACTOR	R.M.S.	PHASE DIFF.	R.M.S.	RESIDUALS AMPL.	PHASE
105.-1*3.	209	K1	53.330	4.183	1.2452	0.0977	-0.097	4.467	4.61	-1.1
207.-22*.	21	EPS2	0.252	0.004	1.1350	0.0169	3.643	0.850	0.02	110.8
233.-236.	10	2N2	0.861	0.004	1.1320	0.0053	3.363	0.266	0.06	114.4
237.-23*.	10	MU2	1.005	0.004	1.1932	0.0044	4.112	0.211	0.08	70.7
245.-245.	13	N2	6.741	0.004	1.1730	0.0007	3.187	0.033	0.38	80.4
246.-248.	11	NU2	1.277	0.004	1.1700	0.0036	2.662	0.176	0.06	81.0
252.-258.	26	M2	35.757	0.004	1.1911	0.0001	2.467	0.006	1.78	59.7
262.-264.	5	LAM2	0.255	0.004	1.1437	0.0173	3.427	0.862	0.02	105.1
265.-267.	12	L2	0.959	0.003	1.1425	0.0033	2.505	0.164	0.05	110.5
271.-272.	2	T2	0.934	0.004	1.2021	0.0046	1.128	0.216	0.04	29.6
273.-275.	4	S2	16.902	0.004	1.2102	0.0003	1.132	0.013	0.77	25.6
274.-277.	12	K2	4.587	0.003	1.2070	0.0008	1.202	0.039	0.20	28.5
282.-285.	15	ETA2	0.253	0.003	1.1834	0.0141	-0.142	0.678	0.01	-5.9
292.-295.	14	2K2	0.072	0.002	1.2348	0.0358	-1.943	1.593	0.01	-19.4
327.-375.	17	M3	0.402	0.010	1.0788	0.0264	0.172	1.393	0.03	2.2
111.-111.	3	SM1	0.0031	0.0012	0.31	0.12	256.77	22.96	0.01	-166.4

STANDARD DEVIATIONS SM 0.51

References.

Aldridge, K.D. and Lumb, L.I., 1988. On the nature of long period gravimetric data from the Earth's fluid outer core. Manuscript : 1 - 4.

Gunn, S. and Aldridge, K.D., 1988. Inertial waves in a differentially rotating fluid. Structure and Dynamics of Earth's Deep Interior AGU Geophysical Monograph 46. IUGG Volume 1, 51 - 54

Melchior, P. and Ducarme, B. 1986. Detection of inertial gravity oscillations in the Earth's core with a superconducting gravimeter at Brussels. Phys. Earth Planet. Int., 42 : 129 - 134.

Melchior, P., Crossley, D.J., Dehant, V.P. and Ducarme, B., 1988. Have inertial waves been identified from the Earth's core. Structure and Dynamics of Earth's Deep Interior AGU Geophysical Monograph . IUGG Volume 1, 1 - 12.

Venedikov, A.P., 1966. Une méthode pour l'analyse des marées terrestres à partir d'enregistrements de longueur arbitraire. Observatoire Royal de Belgique, Comm. N° 250, S. Géophysique N° 71 : 437 - 459.

Venedikov, A.P., 1978. Analysis of Earth tide records (in Russian). Study of the Earth tides, KAPG, Bull. N° 1, Budapest.

Table IV

Filters length	36		42	
Periods	Amplit.	R.M.S.	Amplit.	R.M.S.
h				
13.918	7.6	± 5.8		
13.924	14.9	5.6	13.0	± 6.2
14.066	2.9	8.1	7.2	5.3
14.228	20.6	13.9	16.3	14.4
14.394	10.6	7.6		

The unit of the amplitudes is nanogal.

COMPUTATION OF TIDAL DISPLACEMENTS BY MEANS OF A PERSONAL COMPUTER.

B. Janssen *, B. Ducarme
Royal Observatory of Belgium
Avenue Circulaire, 3
B-1180 BRUSSELS

1 Introduction

At present, the calculation-power of personal computers is sufficient to carry out a harmonic synthesis that is up to standard concerning tidal displacements.

The fortran-programs MT1 and MT2 are greatly simplified versions of the programs MT81 and MT811 that have existed for over ten years at the Royal Observatory of Belgium. This simplification should bring about a wider use of tidal displacement data by related (non-specialized) disciplines such as geodesy.

- Program MT1 calculates the displacements due to body tides.
- Program MT2 calculates the displacements due to body tides plus the Loading effect.

The Loading effect cannot as yet be computed by a personal computer due to the vast amount of data required by the Farrell- algorithm of convolution over the world's oceans. The amplitudes and phases of the loading effect therefore have to be computed by a computer at least capable of handling magnetic tapes. The output can then be used as input for MT2.

The abridged formulas that have been applied are given here.

2 Synthesizing the tidal potential

The tidal potential is the source of all observable quantities such as displacements.

It would have been quite easy to derive the tidal displacements directly from the positions of moon and sun but this implies that information about frequencies of tidal components is not extracted; a division into families and groups cannot directly be carried out. If we consider the elastic response of the earth to the tidal forces, we would be able to apply only a global factor accounting for the response to the tidal force.

*Technische Universiteit Delft, Faculteit der Geodesie. Thijsseweg 11, NL-2629 JA Delft.

Information about occurring tidal frequencies is indispensable when considering the oceanic Loading effects that are very much frequency dependent.

In the aforementioned programs the expansion of the potential into tidal constituents by Cartwright, Tayler and Edden is applied. (Cartwright & Tayler, 1971, Cartwright & Edden, 1973).

In order to find tidal displacements at a certain location and time the tidal components have to be (re-)synthesized according to a recipe that differs for each derivative of the potential. (such as displacements, forces, inclination of vertical, a.s.o.).

The synthesis is $W_n = \sum_k \text{wave}_k$ where

$$(1)\ \text{wave}_k = \text{amp}_k \cdot \frac{g_{nm}(\phi)}{max|g_{nm}(\phi)|} \cdot \begin{array}{l} D_n.\cos\left[a_k\tau + b_k s + c_k h \right. \\ \left. +\ d_k p + e_k N' + f_k p_s + n_k.90^o\right] \end{array}$$

where

- amp_k is the astronomical amplitude of the wave with index k.
- $g_{nm}(\phi)$ is the geodetic function of order n and degree m.
- $\max|g_{nm}(\phi)|$ is Doodson's normalization factor. Every family of waves is multiplied by a different geodetic function. By normalizing it is obtained that the (maximum) amplitudes of waves in different families are still directly comparable.
- D_n is Doodson's constant for order n for either sun or noon. (Ducarme, 1989)
- $a_k\tau + b_k s + c_k h + d_k p + e_k N' + f_k p_s + n_k.90^o$
  is the wave's argument (or phase).

$$a_k, b_k, c_k, d_k, e_k, f_k$$

are the constituents of the argument number according to Doodson.

τ	: hour-angle of moon (or sun)
s	: mean longitude of the moon
h	: mean longitude of the sun
p	: longitude of the moon's mean perigee
N'	: negative longitude of the moon's mean mode
p_s	: longitude of the sun's mean perigee.

$n_k.90^o$ is to "convert" the cosine in (2) into a sine-function. In Fourier-analysis summations of both sines and cosines appear whilst (2) only has a cosine at its disposal. Nevertheless, sines do appear in the development. If this is the case for a particular wave, a 90^o -shift is added so that the (standard-) cosine will yield the same value as if there were a sine. It can be shown that n_k = 0 if (n+m) is even and n_k = -1 if (n+m) is odd.

3 Synthesizing displacements

Displacements in the local frame (positive towards vertical, cq. south, cq. east) are derived from the potential.

$$(2a) \quad u_r = \sum_{n=2}^{\infty} H_n \frac{W_n}{g},$$
$$(2b) \quad u_\theta = -\frac{1}{g} \sum_{n=2}^{\infty} L_n \frac{\partial W_n}{\partial \phi},$$
$$(2c) \quad u_\lambda = \frac{1}{g} \sum_{n=2}^{\infty} L_n \frac{\partial W_n}{\cos\phi \partial \lambda},$$

ϕ is the latitude (zero at the equator; positive towards the poles), λ is the longitude (positive towards the east).

H_n is the Love number for vertical displacements,
L_n is the Love number for lateral displacements.
W_n is the tidal potential of the order n
(Melchior, chI, 1983).

For the horizontal components the factor 1/g is introduced into the Doodson's constant.

Second order:

$$(3a) \quad D_2(r).(1/g) = D_0 \left[\frac{r_A}{\overline{a}}\right]^2 . \frac{1}{g} \text{ (for second order potential)}$$
$$= D_0 \left[\frac{a(1-e.\sin^2\phi + h/a)}{\overline{a}}\right]^2 . \frac{1}{g}$$
$$= 0.268\,462(1 - e.\sin^2\phi + h/a).^2(981/g) \text{ meter}$$
$$= 26.846\,2(1 - 3.35289.10^{-3}\sin^2\phi + h/6378.16)^2(981/g)\ cm$$

where $r_A = a.(1 - e.\sin^2\phi + h/a)$
= geocentric distance to observation point A,

a = radius of the equator,
$\overline{a}$ = mean radius of the Earth $\Big\} \left[\frac{a}{\overline{a}}\right] = 1.002241$

h = height over the ellipsoid in km

Third order:

$$(3b) \quad D_3(r).(1/g) = D_2(r).(1/g).\frac{r_A}{a}$$
$$= D_2(r).(1/g).(1 - e.\sin^2\phi + h/a]$$

For the horizontal components the derivation $\frac{1}{g}.\frac{\partial W}{\partial \phi}$ will convert the geodetic function and the argument will be converted by the derivation $\frac{1}{g}.\frac{\partial W}{\cos\phi\ \partial\lambda}$ affecting the hour-angle HA intervening in W_n.

After derivation and introduction of Doodson's normalization factors the normalized geodetic functions

$$\gamma^a_{nm}(\phi) = \frac{g^a_{nm}(\phi)}{|max\ g_{nm}(\phi)|}$$

become:

(4)

	Long-Period	Diurnal	Semi-diurnal
V	$\frac{1}{2}(1-3\sin^2\phi)$ *	$\sin 2\phi\cos(HA)$	$\cos\phi^2\cos(2HA)$
N-S	$\frac{3}{2}\sin 2\phi$ †	$-2\cos 2\phi\cos(HA)$	$\sin 2\phi\cos(2HA)$
E-W	0 ‡	$2\sin\phi\sin(HA)$ §	$2\cos\phi\sin(2HA)$

This is logical: the east-west force reaches its peak when the moon is at the horizon, the V and N-S forces are minimal then. (And vice versa when the moon transits the local meridian).

Obviously, the geodetic coefficients are different for each axis now. This leads to an individualization of the notation for geodetic coefficients for displacements $g^a_{nm}(\phi)$. (n order, m degree, a axis).

The same is valid for the displacements ($\Rightarrow u^a$).

If it is desired to calculate the displacement in intervals of Δt hours, the linearity of the basic arguments τ, s, h, p, N', p_s comes in very handy.

If we write $t_i = t_0 + i\Delta t$ then

(5a)
$$u^a(t_i) = \sum_k amp_k.\gamma^a_{nm}(\phi).D_n.\cos\{arg(t_0 + i\Delta t)\}$$

or

(5b)
$$u^a(t_i) = \sum_k amp_k.\gamma^a_{nm}(\phi).D_n.\cos\{arg(t_0) + i\omega_k.\Delta t\}$$

where $arg_k(t_0) = a\tau + bs + ch + dp + eN' + fp_s = \omega_k t_o$
$\omega_k = a\dot{\tau} + b\dot{s} + c\dot{h} + d\dot{p} + e\dot{N}' + f\dot{p}_s$(angular velocity),

For computing purposes, this expression is a blessing, as

(5c) $\cos(arg_k(t_i)) = \cos\{arg_k(t_0) + \omega_k.i\Delta t\}$
$= \cos(arg_k(t_0)).\cos(\omega_k.i\Delta t) - \sin(arg_k(t_0)).\sin(\omega_k.i\Delta t)$

This implies that it is sufficient to calculate
- $\cos(arg_k(t_0))$and $\sin(arg_k(t_0))$for every wave k (this means, on its turn, that Brown's and Newcombs's formulas only are evaluated for t_0),
- $\cos(\omega_k\Delta t)$and $\sin(\omega_k\Delta t)$for every wave k.
$\cos(arg_k(t_i))$can be iterated by means of (5c).

---

* $g_{20}(\phi) = 3(\sin^2\phi - \frac{1}{3})$, $max|g_{20}(\phi)| = 2$ $\Rightarrow$ $\frac{g_{20}(\phi)}{max|g_{20}(\phi)|} = \frac{3}{2}(\sin^2\phi - \frac{1}{3})$

† $-\frac{\partial g_{20}}{\partial\phi} = \frac{3}{2}\sin 2\phi$

‡ $\frac{\partial g_{20}}{\partial\lambda} = 0$ (The zonal potential does obviously not produce any east-west forces nor displacements).

§ $\frac{\partial\cos(H(A))}{\partial\lambda} = -\sin(H(A))$, the sine will be replaced by $\cos(H(A) + 90°)$. In other words, a 90° -phase-shift is applied.

4 Loading

The indirect or Loading effect is the flexure of the earth's crust caused by the variable weight of the ocean. This variation is of course caused by the oceanic tides.

The Loading effect has a particular phase and amplitude. The harmonic dial is very suitable to depict the behaviour of waves of a particular frequency.

The "period of the clock" corresponds to the period of the wave (eg. 12 lunar hours for M_2). The long hand points at the time of maximum displacement (eg. lunar transit for M_2), its length is proportional to its amplitude. The small hand corresponds to the Loading effect. It is evidently out of phase. The total effect is found by vectorial addition.

In order to calculate the loading effect, the oceans have been divided into (1^o x 1^o) squares. The mean amplitude and phase of the oceanic tide in these squares has been found by solving the differential equations ruling the fluid motion. These amplitudes and phases can be represented by harmonic dials distributed over a stretch of ocean. (fig. 2). An amphidrome and cotidal lines are sketched to illustrate the interconnection between cotidal charts and (discrete) representation over (1^o x 1^o) squares.

The "hand" or vector representing Loading at station A is found by the convolution summation over the whole ocean

(6) $\overline{L}_A(amp,\ phase) = \sum_\phi \sum_\lambda \mathcal{G}\,(\vartheta_{AQ})\,\overline{\xi}_Q\,\rho\,\Delta\sigma_Q$ (Farrell, 1972)

where $\mathcal{G}(\vartheta_{AQ})$ is Green's function marking the flexure caused by a load of 1 kg over a spherical distance of ϑ_{AQ} degree between station A and square Q.

$\overline{\xi_Q}$ is the tidal amplitude and phase when maximum is reached in square Q.

ρ is the density of seawater

$\Delta\sigma_Q$ is the surface of square Q.

Unfortunately, oceanographers use some peculiar definitions: they refer the phase of an oceanic wave to the upper transit of the mon at Greenwich and regard lags as positive whilst others refer to the local transit of the moon and refer to lags as negative.

This yields the relationship

(7) $\Lambda = -X - m.\lambda$ where Λ : earth tides phase lag
X : oceanic tide phase lag
λ : longitude.

Moreover, if the geodetic coefficients are negative, the body tide vector is orientated inversely. Since oceanographers did not adapt this, 180^o (or 270^o in case of east-west displacement) has to be added to the Loading vector.

The Loading vectors can be computed only for the eleven tidal constituents considered by Schwiderski (1980):

$$Q_1,\ O_1,\ P_1,\ K_1,\ N_2,\ M_2,\ S_2,\ K_2,\ M_f,\ M_m,\ S_{sa}$$

On the other hand the 505 waves of the Cartwright-Tayler-Edden development are usually in groups with close angular velocity.

For the waves given by Schwiderski we have to make a vectorial composition between the body tides displacement vector ($\overline{u}(u_r, o)$, $\overline{v}(u_\vartheta, o)$, $\overline{w}(u_\lambda, \frac{\pi}{2})$ and the corresponding loading displacement vector ($\overline{L}_u(L_u, \Lambda_u)$, $\overline{L}_v(L_v, \Lambda_v)$, $\overline{L}_w(L_w, \Lambda_w)$).

The resulting vectors are shown in figure 1 as

$$\overline{U}(f_u\, u_r, \alpha_u),\ \overline{V}(f_v\, u_\theta, \alpha_v),\ \overline{W}(f_w u_\lambda, \alpha_w)$$

the f_i are considered as modelized amplitude factors and the α_i as modelized phase differences. They will be applied to all the waves belonging to the corresponding group.

5 Summary of the calculation procedure

- read from a dataset the waves' amplitudes and argument numbers. (e.g. Cartwright, Tayler and Edden)
- calculate the angular speeds of the waves ω_k
- calculate D_n
- calculate $g^a_{nm}(\phi)$
- adapt amplitude and phase for Loading
- calculate the initial astronomical argument of the waves:
  $arg_k = a_k\tau + b_k s + c_k h + d_k p + e_k N' + f_k p_s + n_k.90^o$
  (using Brown's and Newcomb's formulae)
- calculate $u^a_k(t_o)$
- add up; $u^a = \sum_k u^a_k$

reiterate from argument computation using recurrence formula 5.

6 Results

Displacements can be calculated in the local frame vertical, South, East. Program MT2 will include the loading effect. MT1 will not. Therefore the loading effect can easily be derived by comparing results. The load vectors are computed from Schwiderski (1980) maps by means of Farrell algorithm (1972).

Displacements expressed in the geocentrical cartesian frame are useful for calculating eg. the dilatation of a baseline. This can easily be done by projecting the vectorial displacements of two stations onto the baseline and finding the differences.

Tidal Loading Displacements at Brussels (cm)

1-19	Ssa	L^r	Λ^r	L^θ	Λ^θ	L^λ	Λ^λ
20-46	Mm						
47-74	MF	.069	-2.25	.008	167.00	.015	22.99
75-105	MTM						
106-128	MQM						
129-193	Q1	.005	95.17	.004	-52.65	.004	-178.18
194-219	O1	.083	88.53	.023	-128.44	.025	159.38
220-241	NO1						
242-251	P1	.068	58.61	.008	136.61	.014	90.84
252-274	K1	.222	55.93	.029	133.61	.039	74.85
275-296	J1						
297-333	OO1						
334-374	2N2						
375-398	N2	.122	69.69	.032	153.10	.043	118.54
399-424	M2	.635	59.94	.163	141.71	.253	98.38
425-438	L2						
439-447	S2	.200	29.25	.056	106.30	.076	60.94
448-488	K2	.041	36.35	.015	99.79	.021	73.05
489-505	M3						

References

[1] Cartwright D.E., Tayler R.S., *1971: New computations of the tide generating potential.* Geophysical Journal, Royal Astr. Soc., 23, 45-74.

[2] Cartwright D.E., Edden A.C., *1973: Corrected tables of tidal harmonics* Geophysical Journal, Royal Astr. Soc., 33, 253-264.

[3] Ducarme B., *1989: Tidal potential developments for precise tidal evaluation.* Bull. Inf. Marées Terrestres, 104, 7338-7360.

[4] Farrell W.E., *1972: Deformation of the Earth by surface loads.* Reviews of Geophys. and Space Physics, 10, 3, 761-797.

[5] Melchior P., *1983: The Tides of the planet Earth.* Pergamon Press, 2nd edition, 641 pp.

[6] Schwiderski E.W., *1980: On charting Global Ocean Tides.* Review of Geophys. and Space Physics, 18, 243.

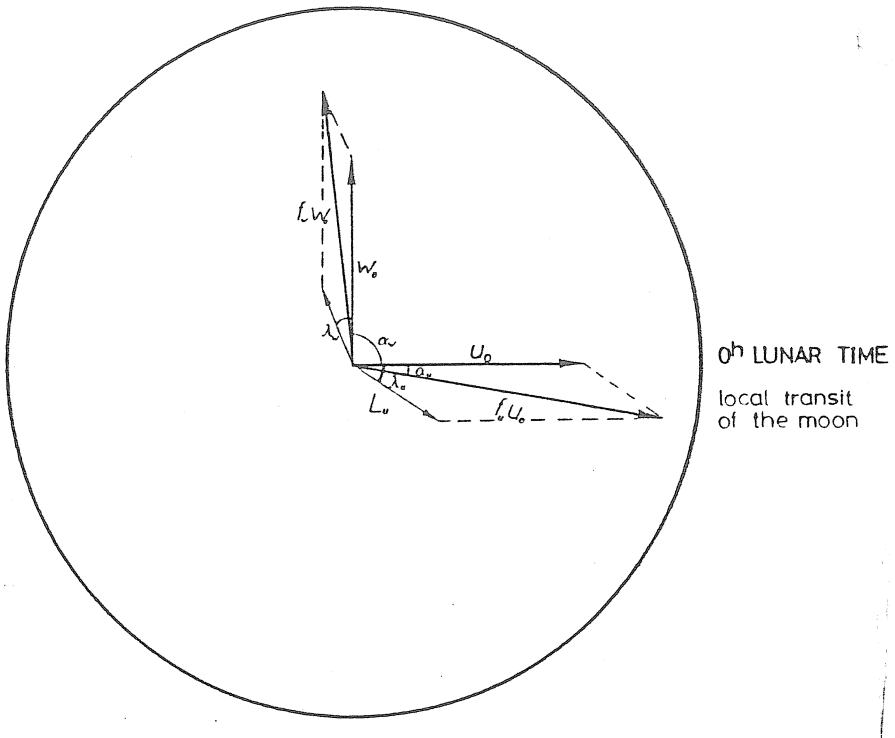

Figure 1: Vectorial addition of direct and indirect effect

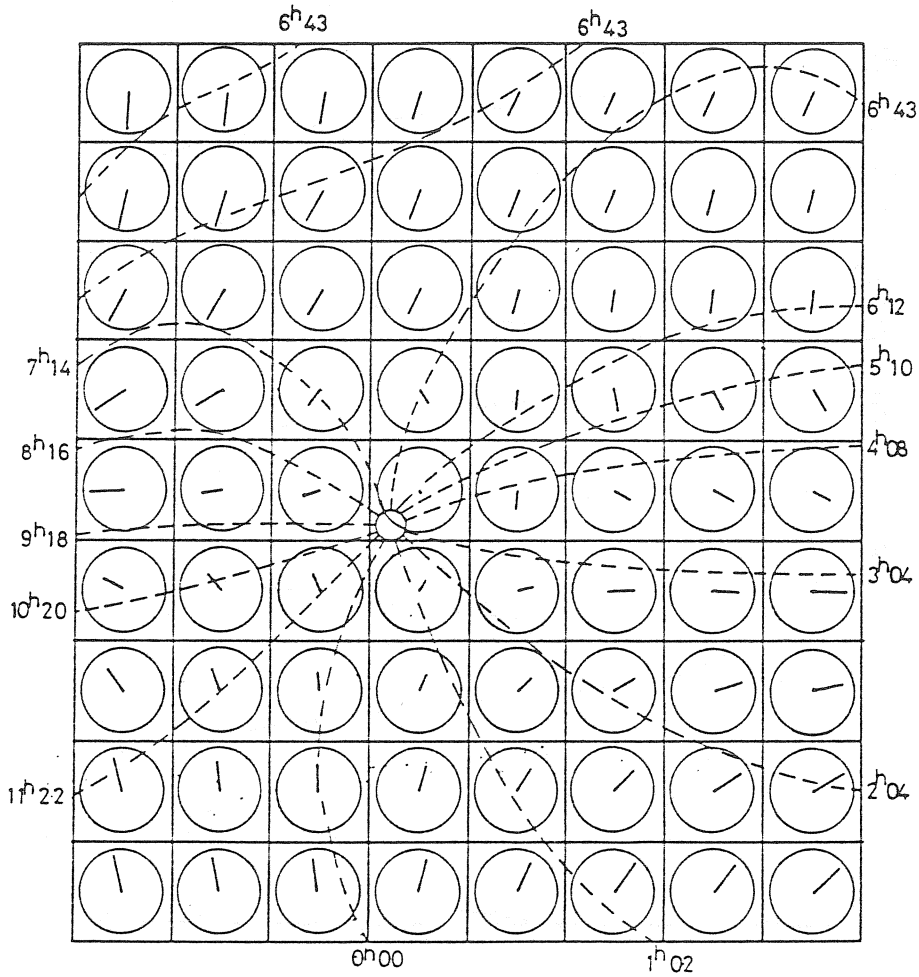

Figure 2: Relationship between the cophase lines and their vectorial representation around an amphidromic point (M_2 tide .)

FIGURE 3.

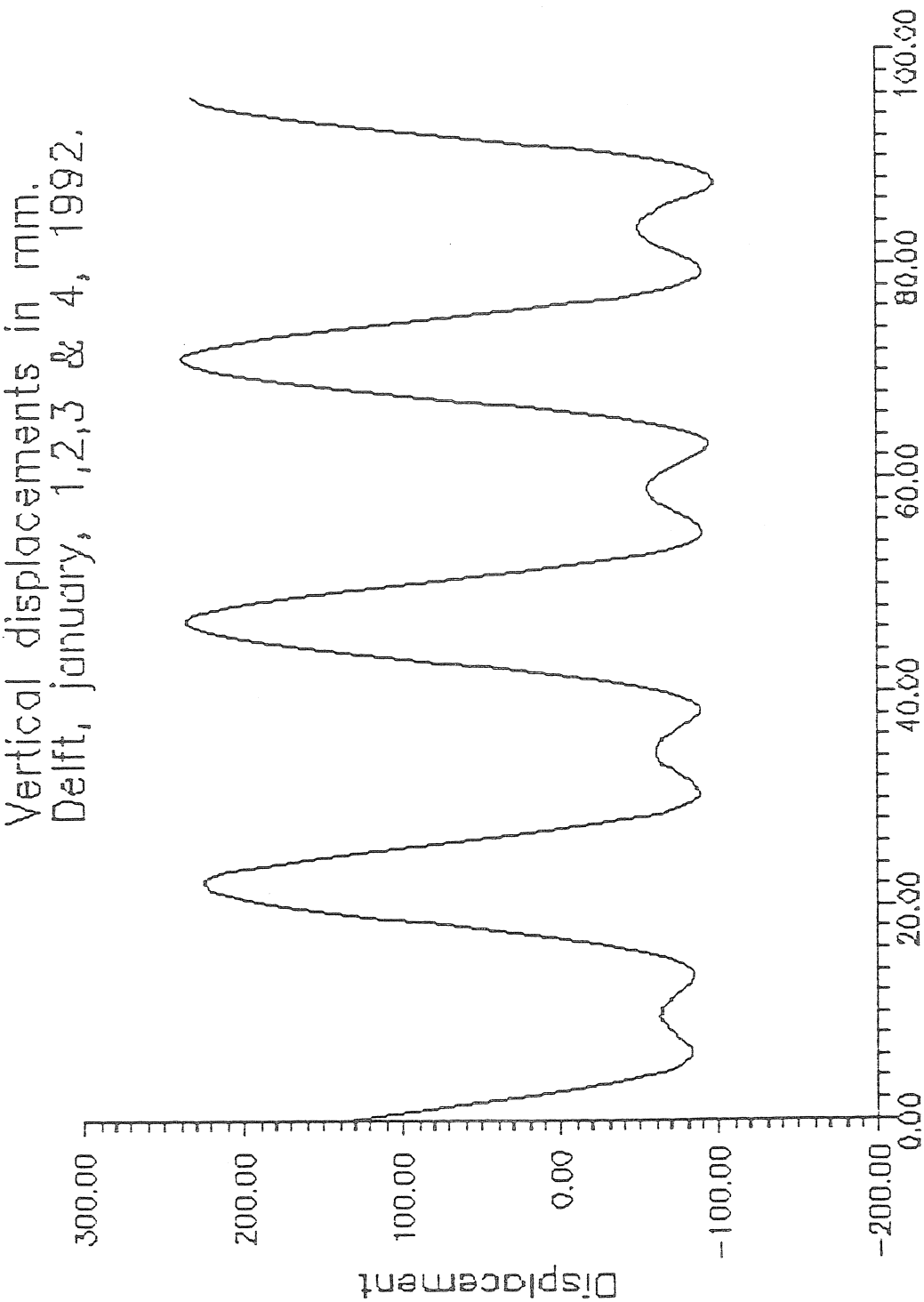
Vertical displacements in mm.
Delft, january, 1,2,3 & 4, 1992.
Displacement
300.00
200.00
100.00
0.00
-100.00
-200.00
0.00
20.00
40.00
60.00
80.00
100.00
Time in hours

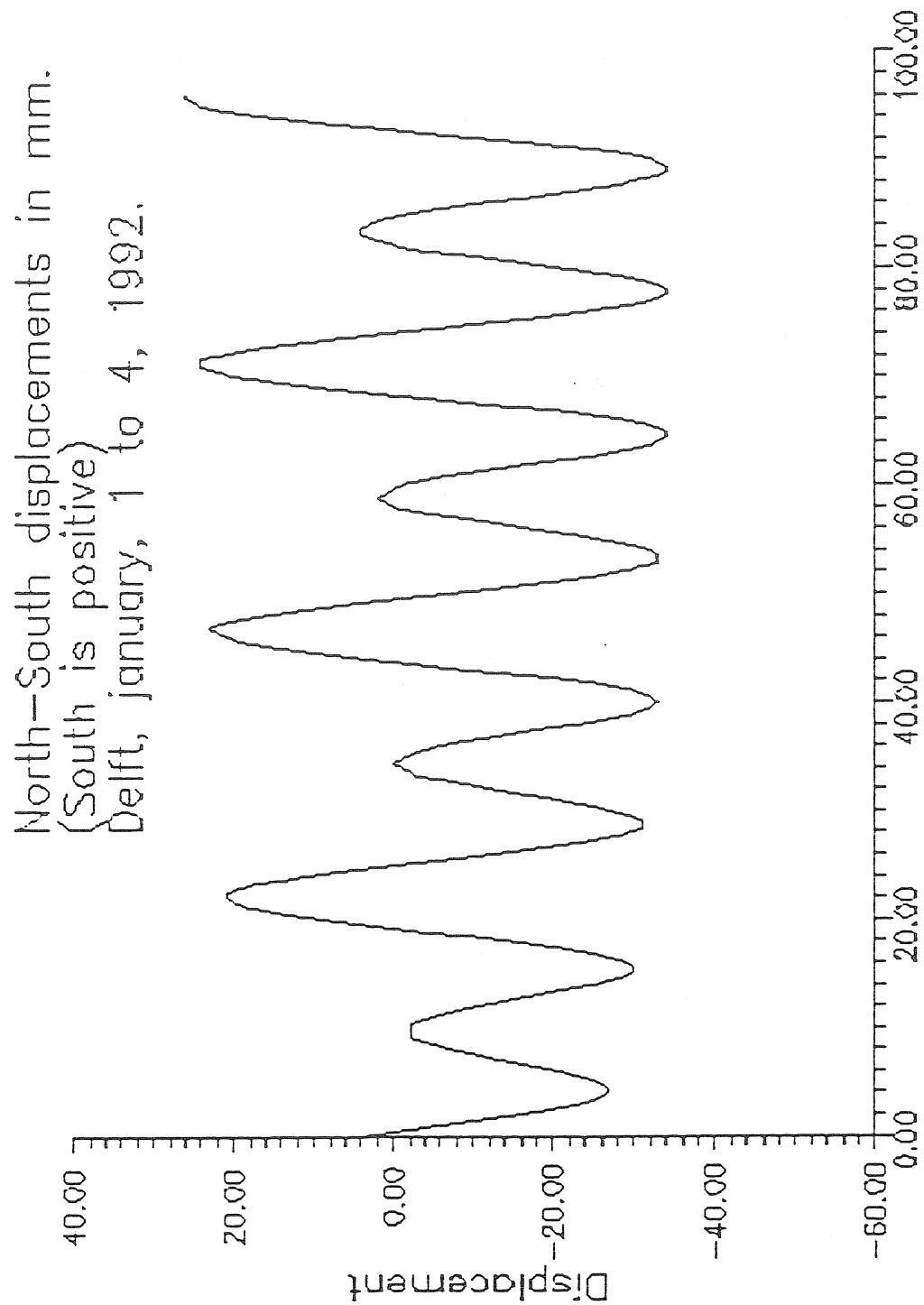
North–South displacements in mm.
(South is positive)
Delft, january, 1 to 4, 1992.
Displacement
40.00
20.00
0.00
-20.00
-40.00
-60.00
0.00
20.00
40.00
60.00
80.00
100.00
Time in hours

FIGURE 4.

FIGURE 5.

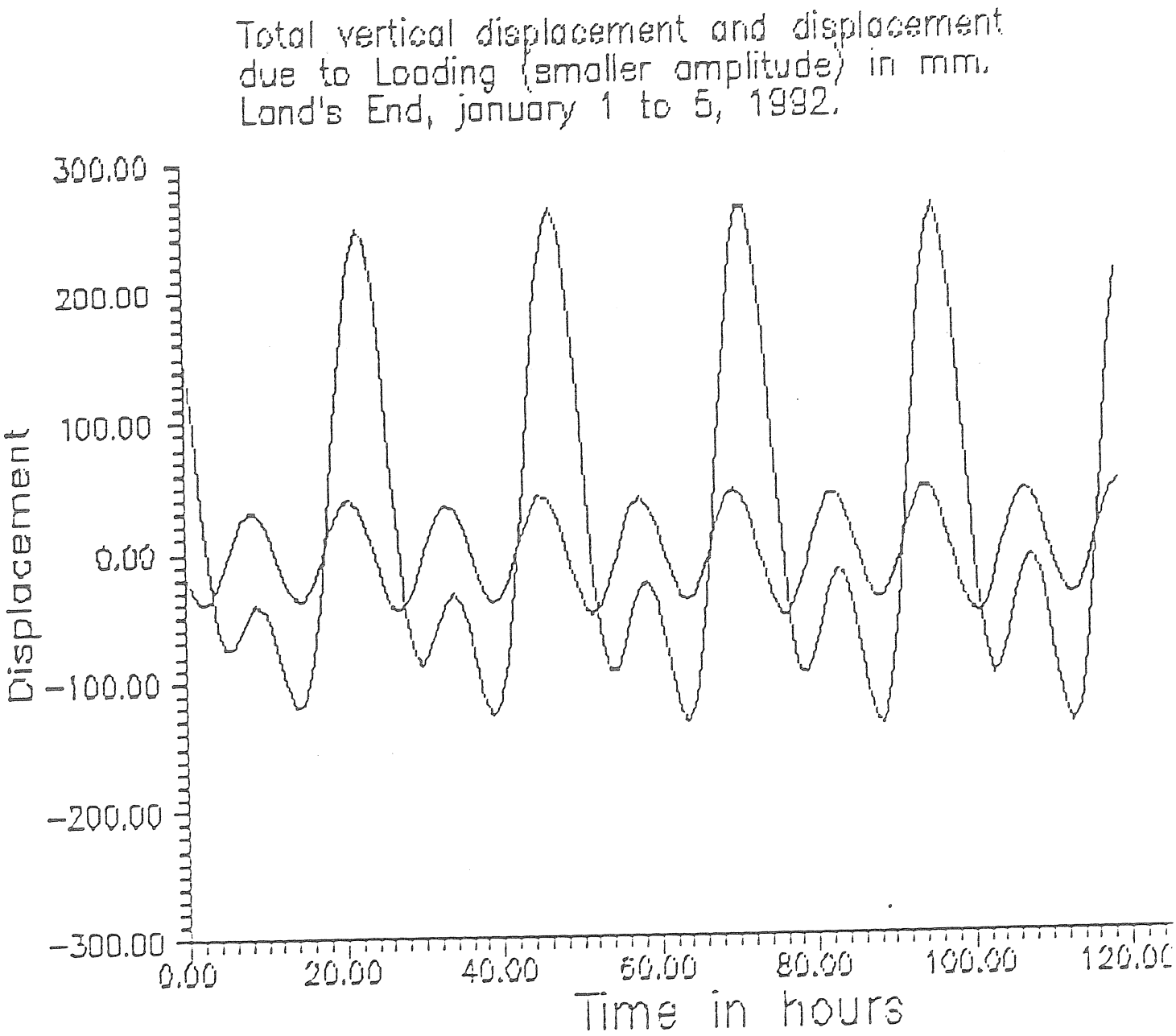
Total vertical displacement and displacement due to Loading (smaller amplitude) in mm.
Land's End, january 1 to 5, 1992.
300.00
200.00
100.00
0.00
-100.00
-200.00
-300.00
Displacement
0.00
20.00
40.00
60.00
80.00
100.00
120.00
Time in hours

FIGURE 6.

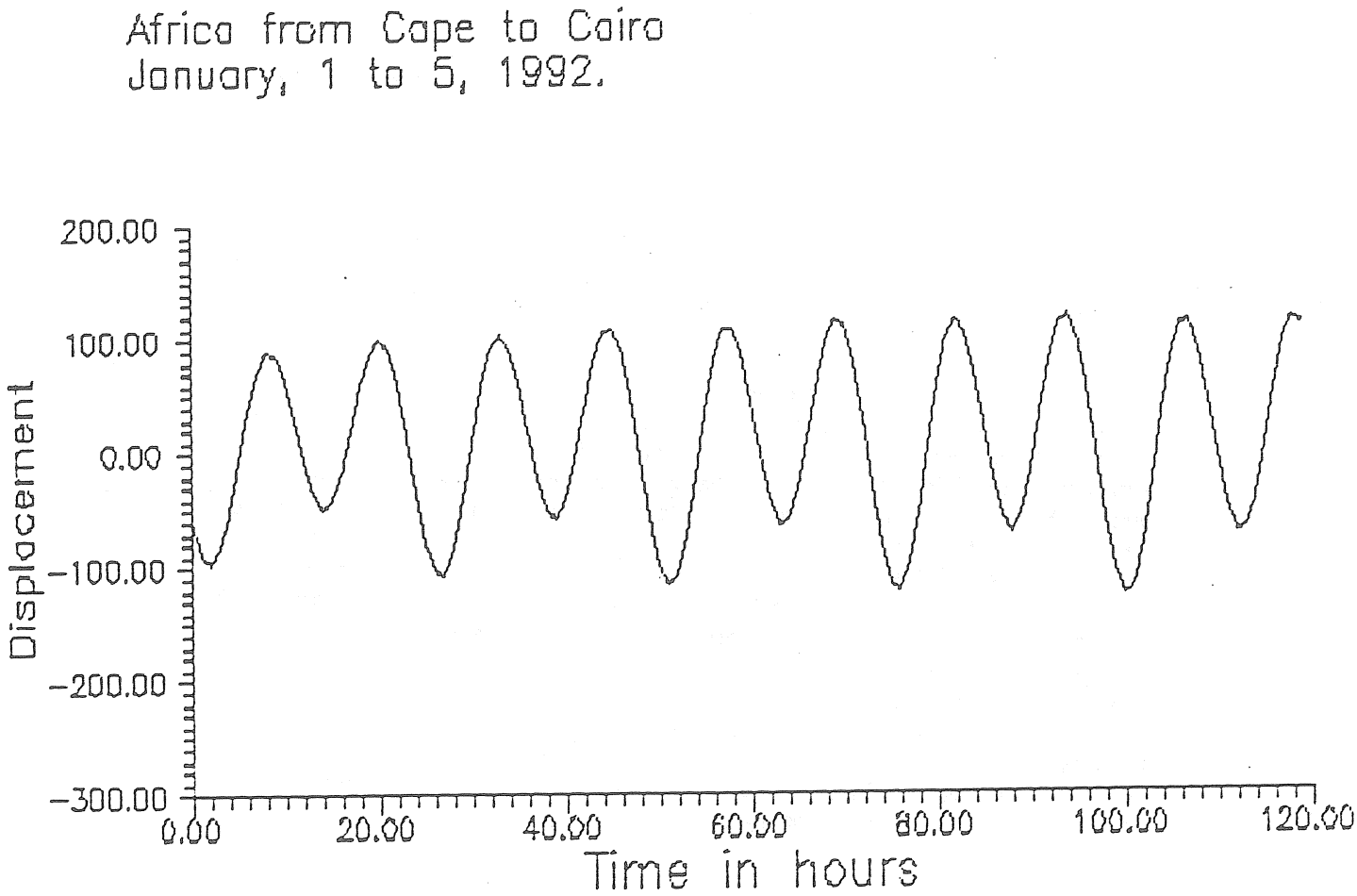
Africa from Cape to Cairo
January, 1 to 5, 1992.
200.00
100.00
0.00
-100.00
-200.00
-300.00
Displacement
0.00
20.00
40.00
60.00
80.00
100.00
120.00
Time in hours

Traduction

Anomalies de marées, flux thermique et séismicité

V. A. Jeligovskii, P. Melchior, A.M. Sadovskii.

Corrélations globales

Problèmes de l'informatique séismologique

Publicat. 21, Moscou Naouka,
pp.32 - 37, 1988.

Cet article est le premier d'une série de travaux que l'on se propose de consacrer à la corrélation de différents champs géophysiques, géodésiques et géologiques à une échelle globale.

On utilise ici trois champs : les anomalies de marées, le flux de chaleur et la séismicité. L'occasion d'un examen de leur corrélation repose sur les résultats du travail [1] où l'on a examiné la répartition globale des anomalies de l'onde de marée M_2 et où l'on a proposé l'hypothèse d'une corrélation de la valeur de l'anomalie avec la mobilité de la lithosphère et de l'asthénosphère. Plus concrètement : les anomalies positives sont rapportées soit aux régions au magmatisme déstabilisé, soit aux systèmes de failles importantes, déstabilisées par les fluides provenant de la croûte, opposées aux régions stables consolidées. Les valeurs absolues des anomalies examinées sont extrêmement faibles - de l'ordre du microgal et moins - c'est pourquoi intervient l'hypothèse que la répartition globale de ces anomalies reflète uniquement des erreurs dans leur détermination.

Le but initial de ce travail était une vérification de l'hypothèse concurrente par comparaison des anomalies de marées avec les autres facteurs indépendants reflétant également la mobilité de la partie supérieure de la Terre (comme facteurs on examine ici le flux de chaleur et la séismicité). Il est évident que des comparaisons semblables présentent aussi un intérêt indépendant. Ainsi, la corrélation trouvée dans le travail [1] est difficilement explicable par des modèles actuels de la lithosphère et, si elle est confirmée, peut servir d'indication sur la nécessité d'un nouvel examen de ces modèles. L'examen préliminaire des trois champs indiqués a été fait en [1] et a donné des résultats prometteurs. Nous étudierons ici plus en détail la valeur statistique de cette corrélation.

Dans le présent travail on a utilisé les données sur les anomalies de marées de la Banque de données créée par le Centre International des Marées Terrestres [2]. La détermination de l'anomalie r est donnée en [1]. Les données sur le flux de chaleur sont tirées de [3], sur la séismicité de [4].

Flux de chaleur et anomalie de marées

Comparaison.

Ces champs sont très souvent mesurés en des points différents. Nous avons comparé l'anomalie de marée r dans chaque station avec la valeur moyenne H des mesures du flux thermique dans un cercle de rayon R = 150 Km autour de cette station. On a vérifié l'hypothèse qu'avec une augmentation des valeurs de r les valeurs H augmentent aussi. La difficulté de vérifier cette hypothèse est liée au fait que s'exerce sur les anomalies de marées et le flux thermique, l'influence d'une série de facteurs géologiques et géophysiques de types différents. Sur les valeurs utilisées ici pour r et H peuvent jouer aussi les erreurs de mesure et les particularités locales des points en lesquels les mesures ont été faites. Ces deux causes obligent à se limiter uniquement à une comparaison fortement robuste de r et de H. Pour cela tout l'intervalle de variation de r a été partagé en valeurs élevées, moyennes et petites de sorte que, dans chaque intervalle, on trouvait à peu près le même nombre de mesures. On a réparti les valeurs de H de façon analogue.
Nous donnons dans la table 1 le nombre de mesures où les valeurs de r et H tombaient dans les intervalles correspondants. Les résultats de la comparaison dépendent fortement des données d'Europe où les observations sur les deux champs sont plus détaillées et dans la plupart des cas plus précises. C'est pourquoi nous avons examiné séparément les données pour l'Europe et pour le restant du monde. Pour les territoires hors de l'Europe on n'a pas réussi à démontrer la valeur statistique de l'hypothèse sur la corrélativité. Apparemment la cause principale de cet insuccès est la grande variation du flux thermique pour les différentes régions du monde où ont été réalisées les mesures. Partant de cette condition et également du fait que pour le territoire européen nous avons obtenu un résultat encourageant, nous avons décidé de limiter nos recherches au territoire continental du continent Asiatique et aux points du territoire Européen d'URSS que nous n'avons pas considérés lors de l'étude du territoire européen.

Table 1

Comparaison des anomalies de marées r (μgal) et du flux thermique H (mwatt/m^2)

Intervalle r	H < 57.0	57.0 < H < 75.0	75.0 < H	Tous les H	Intervalle r	H < 57.3	57.3 < H < 75.5	75.5 < H	Tous les H
		Monde					Europe		
r < -0.06	27	16	11	54	r < -0.07	18	11	7	36
0.06 < r < 0.32	12	20	23	55	-0.07 < r < 0.21	12	10	12	34
0.32 < r	15	19	20	54	0.21 < r	5	14	16	35
Tout les r	54	55	54	163	Tous les r	35	35	35	105

Intervalle r	H < 50.0	50.0 H < 64.0	64.0 < H	Tous les H
		Asie		
r < 0.00	5	3	0	8
0.00 < r < 0.4	3	2	3	8
0.4 < r	1	4	5	10
Tout les r	9	9	8	26

Vérification statistique

On a utilisé des critères statistiques non paramétriques de Wilcoxon et Spearman (voir [6]).

Soient $\{r_1^1, \ldots, r_n^1\}$ et $\{r_1^2, \ldots, r_n^2\}$ les deux choix des valeurs de r correspondant aux petites et grandes valeurs de H. Soit K_i le numéro d'ordre du ième élément du premier choix dans le choix unifié $\{r_1^1, \ldots, r_n^1, r_1^2, r_n^2\}$, classé suivant la croissance, on attribue ainsi aux valeurs de r correspondantes un numéro d'ordre égal à la moyenne de leurs numéros dans le choix unifié.

Conformément à notre hypothèse les valeurs de r dans le choix r^1 doivent être plus petites que les valeurs provenant de r^2. Lors de l'application du critère de Wilcoxon on applique à titre d'hypothèse nulle l'hypothèse sur l'égalité des fonctions de répartition des valeurs r^1 et r^2.
On examine la statistique.

$$x = \left[2 \sum_{l=1}^{n_1} K_l - n_1(n_1 + n_2 + 1) + 1\right] \Big/ \left\{\frac{1}{3} n_1 n_2 (n_1 + n_2 + 1) \times \right.$$

$$\left. \times \left[1 - \frac{1}{n_1 + n_2} \frac{1}{(n_1 + n_2)^2 - 1} \sum_{j=1}^{m} t_j (t_j^2 - 1)\right]\right\}^{1/2}.$$

m est ici le nombre de groupes des valeurs de r comparables, où entrent les éléments des deux choix simultanément : t_j est le nombre de valeurs de r comparables dans ce jième groupe.
Pour $n_1 \to \infty, n_2 \to \infty$ le niveau de valeur atteint dans la réalisation de l'hypothèse nulle est égale asymptotiquement (on utilise un critère unilatéral) :

$$\alpha_r^W = (2\pi)^{-1/2} \int_{-\infty}^{x} \exp(-u^2/2) du.$$

On examine de façon analogue l'hypothèse de la non coïncidence des fonctions de répartition des valeurs de H dans les choix correspondants aux petits et aux grands r. (Le niveau correspondant de valeur atteint est désigné par α_H^W).

Nous examinerons maintenant tout l'ensemble des mesures. Soit dans la paire (r_i, H_i) - qui sont les résultats des mesures au ième point - r_i se trouve à l'endroit K_i^r dans la quantité classée d'après l'accroissement des valeurs mesurées r, et H_i - à l'endroit K_i^H du milieu des valeurs H ainsi ordonnées. On vérifie l'hypothèse de la corrélativité de r et H. Dans le cas d'exactitude de l'hypothèse zéro appliquée à la non dépendance des valeurs accidentelles r et H, le niveau de valeur atteint pour la statistique de Spearman est

$$R = 1 - 6 \frac{\sum_{l=1}^{n} (K_l^H - K_l^r)^2}{n(n-1)(n+1)}$$

lors de l'augmentation du nombre n de paires (r_i, H_i) est égal asymptotiquement à

$$\alpha^{Sp} = (2\pi)^{-1/2} \int_{R\sqrt{n-1}}^{\infty} \exp(-u^2/2)du.$$

Avec une valeur donnée de α l'hypothèse vérifiée s'applique avec le niveau de valeur 1 - α . Les valeurs calculées de α sont données dans la table 2. Elles confirment l'hypothèse sur la corrélation des paramètres étudiés.

Table 2

Niveau atteint de la valeur de α (%) lors de l'étude de la corrélation de r et H.

Territoire	α^{W}_{r}	α^{W}_{H}	α^{Sp}	Territoire	α^{W}_{r}	α^{W}_{H}	α^{Sp}
	R = 150 km, tous les r				R = 150 km, r pour q > 3		
Monde	0,46	3,25	2,11	Monde	1,38	1,82	2,38
Europe	0,02	0,13	0,10	Europe	0,21	0,21	0,17
Asie	0,03	1,17	5,82		R = 100 km, tous les r		
				Monde	0,18	1,18	0,23
				Europe	0,20	0,35	0,08

Vérifications supplémentaires.

La confirmation statistique de l'hypothèse se maintient si on se limite aux données d'anomalies de marées les plus sûres.

La Banque internationale des marées terrestres assigne aux mesures une caractéristique de qualité Q. Sa détermination est donnée dans le travail [2]. Nous avons partagé conventionnellement les valeurs de Q en quatre intervalles de sorte qu'en chacun se trouve un nombre à peu près égal de stations. Les limites de ces intervalles de Q sont égales à 3, 6, 11. Si on rejette les données les moins sûres ($q \leq 3$) alors l'estimation de valeur de notre hypothèse reste à un niveau assez élevé (table 2). Cependant, si on examine les mesures avec Q > 6 on ne réussit pas à démontrer la valeur de l'hypothèse ce qui est apparemment lié a la quantité insuffisante de données.

Lorsque R diminue jusqu'à 100 Km, le niveau de valeur de l'hypothèse pour l'Europe reste élevé et augmente pour les données mondiales malgré une certaine diminution de la quantité de données expérimentales (cette diminution est d'ailleurs insignifiante; voir table 2).

Répartition géographique

La répartition géographique des points où la corrélation examinée a ou n'a pas lieu, montre que l'hypothèse se confirme totalement et non pour le compte d'une certaine région : la corrélation s'observe dans la plupart des points sur le territoire d'Iran, de Chine et de la partie sud-est de l'Asie.

En Europe la corrélation s'observe pratiquement sur tout le territoire à l'exclusion de deux points dans la région nord de l'Europe, trois dans la région centrale et deux dans la région sud (il y a en tout en Europe 105 points.)

Séismicité et anomalies de marées.

Comparaison.

On a vérifié l'hypothèse qu'avec l'augmentation de la valeur de l'anomalie de marée les paramètres de la séismicité augmentent aussi. Nous avons examiné deux mesures de séismicité : la magnitude maximum M_{max} et la quantité de secousses fondamentales N des tremblements de Terre dont la distance épicentrale à la station de marée ne dépasse pas R. La valeur N a été calculée pour la période de 1964 à 1984, pour les séismes tels que $M \geq 5$ (conformément à la représentation globale du catalogue [4] pour la période donnée), R = 300 Km. Les séismes principaux ont été tirés du catalogue d'après l'algorithme [5]. Les magnitudes maximales ont été prises pour la période de 1920 à 1984. Pour chaque valeur examinée on a séparé comme précédemment en trois intervalles (table 3, 4). Pour les mêmes raisons que dans le paragraphe précédent, nous avons analysé également les données séparément pour l'Europe et pour les autres continents. Ainsi en Europe, R a diminué jusqu'à 100 Km et le seuil en magnitude lors du calcul de N - jusqu'à 3,5 conformément à la précision élevée des observations aussi bien des anomalies de marées que de la séismicité.

La valeur statistique de l'hypothèse a été estimée de façon analogue en appliquant les critères de Wilcoxon et Spearman. L'hypothèse de la corrélativité des paramètres de séismicité et des anomalies de marées se confirme statistiquement. (tables 5, 6)

Table 3

Comparaison des anomalies de marées r et de la magnitude maximale M_{max}.

Intervalle r	M_{max} < < 5,6	5,6 < < M_{max} < < 6,5	M_{max} > > 6,5	Tous les M_{max}
Monde (R = 300)				
r < - 0,08	28	28	23	79
-0,08 <r<0,42	29	24	23	76
0,42 < r	20	17	41	78
Tous les r	77	69	87	233
Intervalle r	M_{max} < < 2,8	2,8 < < M_{max} < < 4,5	M_{max} > > 4,5	Tous les M_{max}
Europe = (R = 100)				
r < - 0,08	15	14	12	41
-0,08 <r<0,20	15	10	10	35
0,20 < r	9	14	18	41
Tous les r	39	38	40	117
Intervalle r	M_{max} < < 6,0	6,0 < < M_{max} < < 7,3	M_{max} > > 7,3	Tous les M_{max}
Monde sans l'Europe (R = 300)				
r < - 0,09	14	14	10	38
-0,09 <r<1,16	16	10	14	40
1,16 < r	10	13	15	38
Tous les r	40	37	39	116

Table 4

Comparaison des anomalies de marées de et du nombre de chocs importants N.

Intervalle r	N ≤ 1	1 < N < 5	5 < N	Tous les N
Monde (M = 5,0 R = 300)				
r < - 0,08	38	19	22	79
- 0,08 <r<0,42	38	18	20	76
0,42 < r	29	12	37	78
Tous les r	105	49	79	233
Intervalle r	N = 0	0 < N < 3	3 < N	Tous les N
Europe (M = 3,5 R = 100)				
r < - 0,08	20	9	12	41
- 0,08 <r<0,20	16	8	11	35
0,20 < r	11	10	20	41
Tous les r	47	27	43	117
Intervalle r	N < 1	1 < N < 15	15 < N	Tous les N
Le Monde sans tenir compte de l'Europe (M = 5,0, R = 300)				
r < - 0,09	13	14	11	38
- 0,09 <r<1,16	14	15	11	40
1,16 < r	12	10	16	38
Tous les r	39	39	38	116

Table 5

Niveau atteint de la valeur de α (%) lors de l'étude de la corrélation de r et M_{max}

Territoire	W α_r	W α_M	α_{SP}
Tous les r			
Monde (R = 300)	0.22	0.70	0.12
Europe (R = 100)	3.68	3.79	0.91
Le monde sans tenir compte de l'Europe (R = 300)	2.40	3.00	0.65
r pour q > 3			
Monde (R = 300)	5.24	10.8	3.09
Europe (R = 100)	6.82	8.53	5.20
Le monde sans tenir compte de l'Europe (R = 300)	8.99	6.02	4.58

Table 6

Niveau atteint de la valeur de α (%) lors de l'étude de la corrélation de r et N.

Territoire	W α_r	W α_N	α_{SP}
Tous les r			
Monde (R = 300, M = 5,0)	0,20	0,92	0,035
Europe (R = 100, M = 3,5)	0,81	3,60	4,83
Monde sans Europe (R = 300, M = 5,0)	6,12	12,0	2,69
r q > 3			
Monde (R = 300, M = 5,0)	5,45	10,07	1,16
Europe (R = 100, M = 3,5)	5,06	6,47	2,54
Monde sans Europe (R = 300, M = 5,0)	14,1	13,5	11,11

Les Vérifications complémentaires de la confirmation statistiques de l'hypothèse sur la corrélation des valeurs de la séismicité et de l'anomalie de marée sont analogues à celles données plus haut (table 5, 6). Comme dans le cas de r et H, l'hypothèse sur l'existence de la corrélation continue à se confirmer avec un niveau de signification assez élevé.

Répartition géographique.

Comme précédemment nous examinerons dans quelles régions notre hypothèse se confirme et dans lesquelles elle est réfutée. La corrélation dans l'ensemble a lieu sur les territoires d'Iran, d'Inde, d'Asie Centrale, du Japon, de l'Asie Sud-Est, de la Nouvelle Zélande et d'une grande partie de l'Afrique. Les contradictions principales à notre hypothèse se rapportent géographiquement aux territoires de la Chine, la Corée, l'Australie de l'Est, Madagascar et le littoral des USA.
Lors de l'examen séparé de l'Europe apparaissent trois contradictions pour l'Europe septentrionale, huit pour l'Europe Centrale et sept pour l'Europe méridionale. De cette façon, on ne peut tirer la conclusion que la présence et l'absence de corrélation des anomalies de marées et des paramètres de séismicité se rapportent à une région particulière.

Conclusion

Les estimations données montrent que la corrélation indiquée en [1] de la répartition géographique des anomalies de marée avec le flux thermique et de la séismicité est significative.
Les auteurs expriment leur reconnaissance à V.Y. Keilis-Borok pour son examen fécond lors de la réalisation de ce travail.

ЛИТЕРАТУРА

1. *Якшин А.Л., Мельхиор П., де Бекер М.* и др. Глобальное распределение приливных аномалий и опыт его геотектонической интерпретации // Численное моделирование и анализ геофизических процессов. М.: Наука, 1987. С. 3–11. (Вычисл. сейсмология; Вып. 20).
2. *Ducarme B.* A data bank for Earth tides // Bull. Inform. Marees Terrestr. 1984. Vol. 91. P. 5963–5980.
3. *Jessop A.M., Hobart M.A., Sclater J.G.* The world heat flow data collection. – 1975. Ottawa: Geotherm. Serv. Canada, 1976. 320 p. (Geotherm. Ser.; N 5).
4. World hypocenters data file, 1885–1984. NEIS-USGS. Menlo Park, 1986.
5. *Keilis-Borok V.I., Knopoff L., Rotvain I.M.* Bursts of aftershocks, longterm precursors of strong earthquakes // Nature. 1980. Vol. 293, N 5744. P. 259–263.
6. *Кендалл М.Дж., Стюарт А.* Статистические выводы и связи. М.: Наука, 1973. 899 с.

Meeting of the KAPG working group II-5.3 "Earth Tides"
at Stara Lesna/CSSR, 19.-22.September, 1989

On air pressure induced vertical displacements of the Earth surface

by

D. Simon and W. Fleischer*

Abstract

Basing on the Boussinesq model the vertical movements of the Earth surface due to the changing air loadings of a circular area with a diameter of 700 km were calculated.
The modellings concern a period of 45 days with 360 different regional loading distributions succeeding one another in time intervals of 3 hours.
Inside this period the difference between the highest and lowest stages of surface level was 1.502 cm. That corresponds to a variation of the average air pressure within the loading area of about 50×10^2 Pa.
Between Jan. 30. 1989 and Feb. 25. 1989 a maximal air pressure difference of 80×10^2 Pa was observed in the same area.
An estimation yielded, that the maximal level variation may reach on amount of 5 cm for the latter period, if the diameter of the loading area considered in the modellings amounts 2000 km.
As a consequence corrections of high precise LASER ranging measurements and tidal gravimeter records with respect to the regional air pressure effects seem to be useful.

1. Introduction

Nowadays the measuring threshold of LASER ranging measurements is situated in the range of centimeters. The modern tidal gravimeters have a measuring threshold of 1 µgal. A gravimetrical effect of this order of magnitude may be produced by a vertical displacement of the Earth surface of 3.2×10^{-3} m.

The task of the here presented paper was to check the diurnal changing, the velocity and the maximal amount of the vertical displacements of the Earth surface due to variations of the regional air pressure loading.

The modellings were made for the Tiefenort station as observation place where a gravimeter is recording since 1985.

---

* Academy of Sciences of the GDR
Central Institute for Physics of the Earth
DDR-1561 Potsdam, Telegrafenberg A17

are used. These numerical values are taken from SIMON, KACZOROWSKI and FLEISCHER /1989/ where the vertical displacements of the Earth surface were determined on the base of two different Earth models. These were the viscoelastic spherical shell Earth model PREM Q12H and, like in the present paper, the half-room model of Boussinesq.

Both the models result for the same regional air pressure distribution similar amounts of the vertical surface displacement, if the numerical values (13) are used for the calculations basing on the Boussinesq model.

However, the parameters (13) are effective values which are valid only for the used circular loading area with a diameter of 700 km.

For larger diameters the comparison with the results of the PREM Q12H model probably yields larger numerical values for the elastic parameters of the half-room.

3. Results

Fig. 2 shows the calculated vertical movements of the Earth surface at the Tiefenort station. The considered loading area is a circle around the station with a diameter of 700 km.

The vertical displacements were calculated for the period 25.1.1961 - 10.3.1961 (45 days) in time intervals of 3 hours, at the meteorological measuring dates 0^h UT, 3^h UT and so on.

In this period the largest vertical displacement was calculated for the measuring date 5.3.1961, 9^h UT, and the smallest one at the 2.2.1961, 15^h UT. The difference between these extreme values is 1.502 cm.

The largest diurnal variation occured in the time interval between 25.1.1961, 18^h and 26.1.1961, 18^h. It reached an amount of 0.497 cm.

In the lower part of fig. 2 the calculated curve of vertical movements was compared with the barograms of 9 real meteorological stations situated near the centre and the boundaries of the loading area.

There is a good correlation between all these curves. A comparison of the phases shows that a W-E stream was predominating during the whole period. The average stream velocity was about 80 km/h.

To enable a comparison of these results with such ones of other models, for instance of the PREM Q12H model, the tables 1 and 2 contain the air pressure data at the fictive stations for both the extreme loading distributions, 2.2.1961, 15^h UT and 5.3.1961, 9^h UT, respectively.

The numbering of the 147 ring sectors and the positions of their centres of gravity referred to a polar coordinate system where the Tiefenort station is located in the origin are as follows

ring sector No	radius r_e/km	angle from East to North φ_e/°	
0- 2	27.6	360(0.5+ n)/3	for n=0,1,2
3- 11	76.2	360(0.5+ n)/9	n=0,1,...,8
12- 26	125.7	360(0.5+ n)/15	n=0,1,...,14
27- 47	175.5	360(0.5+ n)/21	n=0,1,...,20
48- 74	225.4	360(0.5+ n)/27	n=0,1,...,26
75-107	275.3	360(0.5+ n)/33	n=0,1,...,32
108-146	325.3	360(0.5+ n)/39	n=0,1,...,38

4. Estimation of the total effect for an extreme loading variation

An extreme loading variation was observed in the first quarter of 1989 in Middle Europe.
The air pressure decreased from 1040 × 10^2 Pa at Jan. 30. 89 to 960 × 10^2 Pa at Feb. 25. 89.

Basing on the calculations for a loading area with a diameter of 700 km the corresponding vertical movement amounts to about 2.4 cm.

But the horizontal extensions of the meteorological low and high pressure areas are mostly much larger than 700 km, for instance 2000 km and more.

Table 3 shows for a series of different loading situations that the contributions of the 7 circle rings to the total vertical displacement effect are changing slowly with an increasing ring radius.

However it must be considered that

- starting with m = 7 the next circle rings cover partially oceanic areas where the loading effect of air pressure may be compensated by the corresponding changes of water level
- the loading Green function shows increasing values of the elastic parameters with increasing diameter of the considered loading area.

Notwithstanding both the latter facts the assumption seems to be justified that modellings carried out for the mentioned loading variation probably may result an amount of about 5 cm for the vertical movement of the Earth surface if the diameter of the considered circular loading area will be extended to 2000 km.

5. Influences of the tectonic crustal structure on the amount of the vertical movements

Investigations of ocean loading effects led to the assumption that lateral inhomogeneities of the elastic qualities of the Earth's crust and upper mantle amplify the vertical (and tilt) movements of the loaded surface layers (see JENTZSCH, KACZOROWSKI and SIMON /1988/).

Such effects were attributed, in the first line, to the large tectonical weakness zones of global relevance, for instance to the Middle Atlantic rift system.

But we cannot exclude that smaller fault zones, for instance the Oberrheintalgraben or the Elbtallineament show measurable effects of this kind.

First hints on such effects were received from precision levellings carried out by THURM /1974/ in the valley of the Elbe river.

Furthermore the existence of structure influences can may be checked by means of longbase water tube tiltmeters installed at both the borders of a fault zone perpendicularly to its direction.

6. Conclusions

In the paper was shown that the air pressure induced vertical movements of the Earth surface reach amounts of some centimeters. This result leads to the conclusion that routine calculations of the air pressure effect could help to improve the accuracy of LASER ranging measurements.

The correction of tidal gravimeter records concerning atmospheric pressure influences is more complicated due to the attraction of the air masses. There is a remarkable effect of the air masses located in the antipode area. Consequently it is to integrate on the surface of the whole Earth.

Furthermore additional informations on the distribution of the air masses in the radial direction are required.

Considering all this we concluded that partial solutions of the problem seem to be acceptable too if they enable a significant diminishing of the mean errors of the determined tidal waves.

Such a partial solution could be for instance an approximate elimination of the effects induced by the air masses which are located in the regional surroundings of the measuring place.

In this connection we remember on a suitable correction method which was successfully applicated in 1973 for the evaluation of

- tiltmeter records of the Tiefenort station (SIMON /1973/)
- gravimeter records at the Vostok station, Antarctica (SCHNEIDER and SIMON /1973/).

The method based on the similarity of the barograms recorded at the meteorological stations of a relative large area (see Fig. 2).

There are significant correlations between these barograms and the gravimeter or tiltmeter records.

These correlations exist obviously for constituents of both the air pressure and the tidal records too, for instance for the drift components or for short-living waves with the periods of the tidal waves O1 or K1, respectively.

The correction of the tidal records was carried out in several steps of calculation:

step 1: determination of the correlation or regression coefficients for the relations between the mentioned components of tidal records and the barograms including the calculation of the time shifts between them.
step 2: finding out of such a meteorological station where the time shift between the air pressure variation recorded here and the corresponding gravity variation recorded at the gravimeter station is zero.
step 3: multiplication of the mentioned barogram by the corresponding regression factor and subtraction of the resulting data series from the tidal records.
step 4: harmonic analysis of the residual curve.
step 5: comparison of the mean quadratic errors of the tidal waves calculated before and after this correction.

This method of correction requires only a small part of the air pressure data and of the calculation effort connected with the modellings of that kind as described in the present paper.

References

JENTZSCH, G., KACZOROWSKI, M. SIMON, D.: Models for the tidal tilt wave M2(EW) in the zone for the diminished cavity effects.
6th Int. Symp. "Geodesy and Physics of the Earth", Potsdam /1988/, Proc., pp 284-310.

MELCHIOR, P.: Tides of the Planet Earth.
Pergamon Press, Oxford /1978/.

SCHNEIDER, M.M., SIMON, D.: Influence of atmospheric pressure and air temperature fluctuations on tidal observations of gravity in Central Antarctica.
7th Int. Symp. on Earth Tides, Sopron /1973/, Proc., pp

SCHWAHN, W., ELSTNER, C., SAVIN, I.V.: On the modulation of the M2 gravity tide.
6th Int. Symp. "Geodesy and Physics of the Earth", Potsdam /1988/, Proc., pp 334-354.

SIMON, D.: Über Ergebnisse von Neigungsbeobachtungen in Tiefenort.
2th Int. Symp. "Geodesy and Physics of the Earth", Potsdam /1973/, Proc., pp 207-233.

SIMON, D., KACZOROWSKI, M., FLEISCHER, W.: On strain and tilt movements of the Earth surface induced by atmospheric pressure variations.
11th Int. Symp. on Earth Tides, Helsinki, Aug. 1989.

THURM, H.: Das rezente vertikale Bewegungsverhalten der Erdkruste in der Elbtalzone.
Geod. Geoph. Veröff. R. III, H. 35 /1974/, pp 21-35.

fig.1
network of
meteorolog.
stations

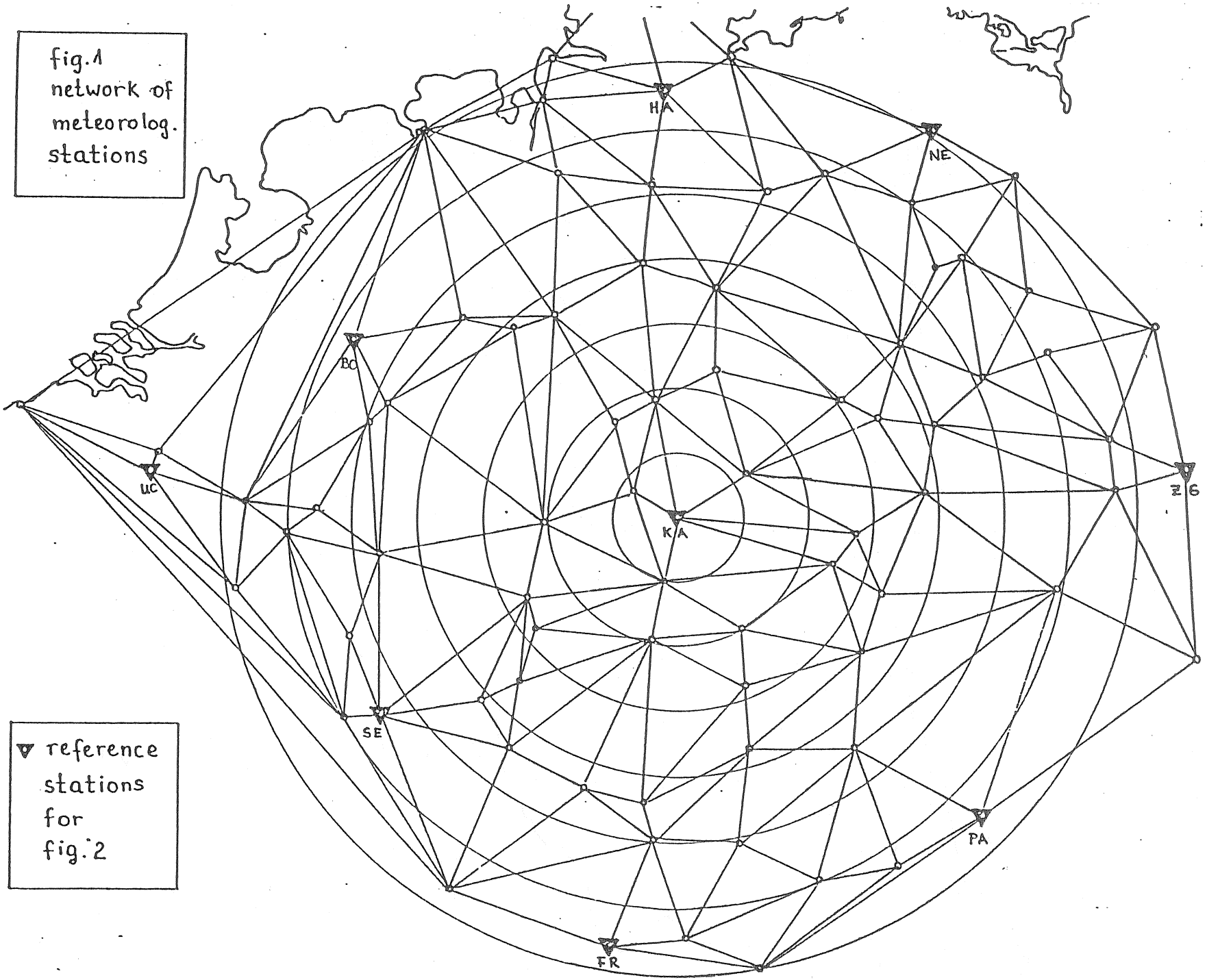

▽ reference
stations
for
fig. 2

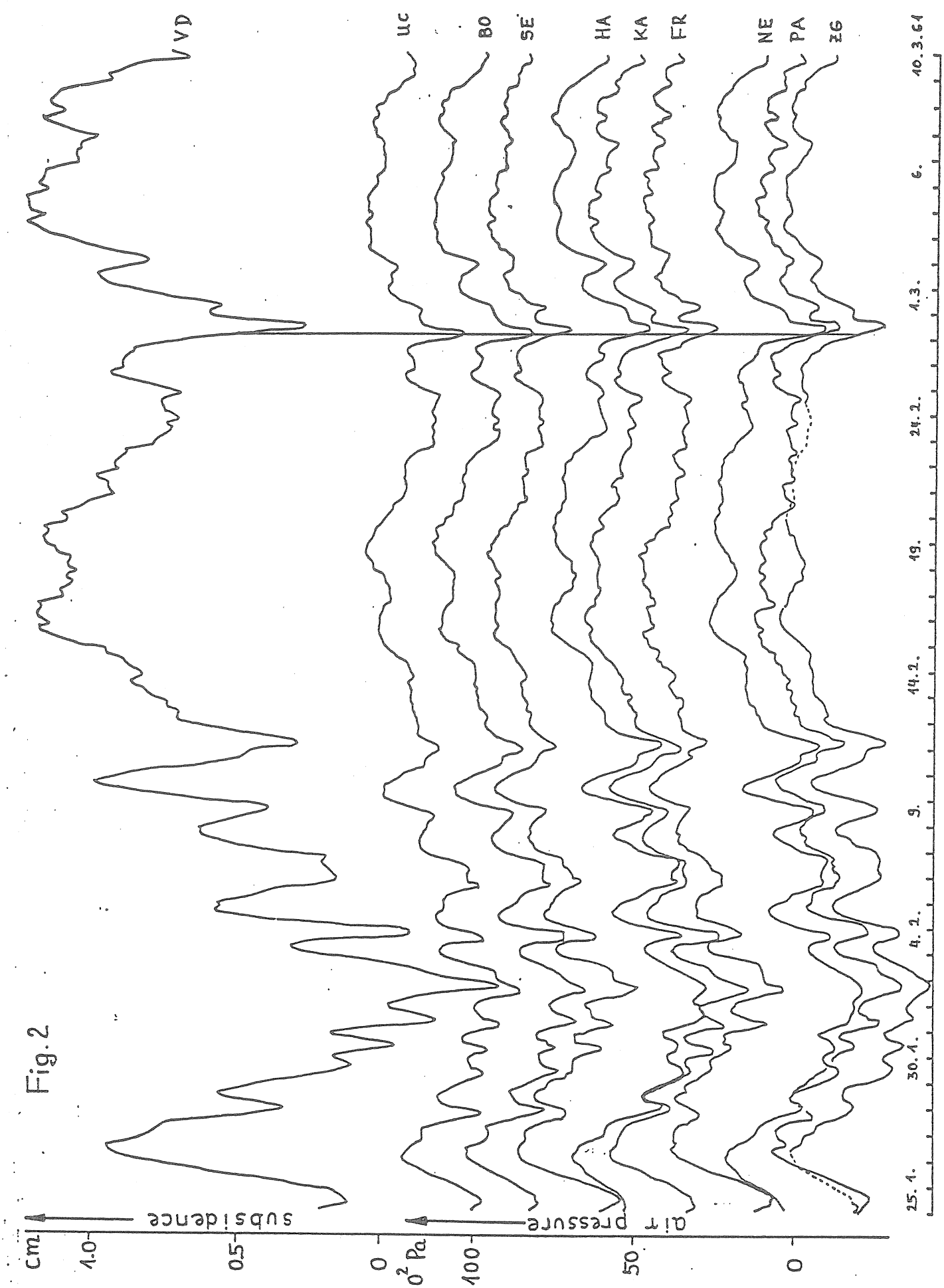
cm
1.0
0.5
0
subsidence
VD
uc
BO
SE
HA
KA
FR
NE
PA
ZG
0^2 Pa
100
50
0
air pressure
15. 1.
30. 1.
4. 2.
9.
14. 2.
19.
24. 2.
4. 3.
6.
10. 3. 64

Fig. 2

table 1 : air pressure distribution 2.2.1961, 15h uT

$\tilde{p} = (A + 900) \times 10^2$ Pa

station №	air press. A	station №	air press. A	station №	air press. A
0	89.02	49	90.27	98	92.03
1	89.18	50	90.36	99	92.31
2	89.19	51	90.05	100	92.36
3	89.18	52	89.70	101	92.73
4	89.06	53	89.48	102	93.12
5	89.01	54	89.28	103	92.81
6	89.56	55	89.38	104	92.80
7	88.99	56	89.69	105	92.66
8	88.87	57	89.90	106	92.08
9	88.92	58	89.73	107	91.61
10	89.32	59	90.23	108	91.67
11	89.10	60	90.39	109	91.55
12	89.59	61	90.25	110	91.39
13	89.72	62	90.01	111	91.38
14	89.47	63	90.03	112	90.36
15	89.18	64	89.72	113	89.86
16	89.41	65	90.14	114	89.23
17	89.61	66	90.71	115	88.80
18	89.52	67	91.01	116	88.46
19	89.06	68	91.30	117	88.41
20	88.73	69	91.34	118	88.73
21	89.11	70	91.78	119	89.26
22	87.96	71	91.99	120	89.73
23	88.42	72	91.84	121	90.06
24	89.43	73	90.53	122	90.36
25	89.59	74	90.92	123	90.63
26	89.09	75	90.91	124	90.87
27	90.01	76	91.13	125	91.10
28	89.99	77	91.03	126	91.29
29	90.02	78	90.06	127	91.42
30	89.70	79	89.95	128	91.70
31	89.34	80	89.67	129	91.90
32	89.64	81	89.33	130	91.96
33	89.80	82	89.35	131	92.42
34	89.88	83	88.89	132	92.41
35	90.24	84	89.27	133	92.30
36	89.71	85	89.71	134	92.65
37	89.63	86	89.98	135	93.06
38	89.38	87	90.10	136	93.34
39	89.25	88	90.29	137	94.83
40	89.46	89	90.46	138	94.68
41	89.31	90	90:55	139	94.23
42	89.66	91	90.09	140	94.41
43	90.12	92	90.97	141	93.81
44	90.47	93	90.77	142	93.51
45	90.80	94	90.69	143	93.48
46	89.13	95	90.96	144	93.32
47	89.67	96	91.40	145	92.98
48	90.30	97	91.75	146	92.23

table 2 : air pressure distribution 5.3.1961, 9^h UT

$\tilde{p} = (A + 900) \times 10^2$ Pa

station No	air press. A	station No	air press. A	station No	air press. A
0	139.36	49	137.96	98	140.30
1	140.77	50	137.83	99	140.71
2	140.60	51	137.69	100	141.38
3	139.55	52	137.68	101	141.53
4	138.62	53	137.61	102	141.74
5	139.60	54	137.62	103	141.11
6	140.09	55	137.95	104	140.14
7	140.23	56	138.16	105	139.14
8	140.43	57	138.55	106	138.19
9	140.79	58	138.82	107	138.47
10	140.30	59	138.95	108	138.27
11	140.50	60	139.17	109	137.33
12	139.29	61	139.28	110	136.92
13	138.61	62	139.45	111	136.78
14	138.37	63	139.54	112	136.82
15	138.75	64	139.74	113	136.69
16	139.11	65	139.81	114	136.56
17	139.31	66	140.19	115	136.71
18	139.84	67	140.09	116	136.96
19	139.89	68	140.42	117	137.19
20	140.08	69	141.30	118	137.35
21	140.01	70	141.34	119	137.51
22	140.84	71	141.02	120	137.79
23	140.86	72	140.25	121	138.15
24	141.43	73	138.30	122	138.44
25	139.91	74	138.57	123	138.65
26	140.15	75	138.48	124	138.95
27	139.01	76	137.81	125	139.34
28	138.69	77	137.44	126	139.81
29	138.20	78	137.18	127	140.26
30	138.15	79	137.23	128	139.89
31	138.25	80	137.17	129	139.32
32	138.40	81	137.19	130	139.43
33	138.53	82	137.03	131	139.36
34	138.83	83	137.51	132	139.38
35	139.54	84	137.67	133	139.32
36	139.50	85	137.92	134	139.63
37	139.58	86	138.35	135	139.86
38	139.76	87	138.43	136	140.18
39	139.92	88	138.33	137	141.70
40	140.45	89	138.55	138	141.79
41	140.47	90	139.33	139	141.54
42	140.30	91	139.01	140	142.15
43	140.43	92	139.74	141	141.54
44	141.05	93	140.21	142	140.58
45	141.33	94	139.45	143	139.79
46	138.65	95	139.38	144	138.98
47	139.06	96	139.46	145	138.18
48	138.53	97	139.95	146	138.46

table 3: contribution of each loaded circle ring to the vertical displacement at its centre

ring No	measur. date	contribut. ΔS_z / cm	measur. date	contribut. ΔS_z / cm
0		0.48459		0.49067
1	24.1.61	0.48516	29.1.61	0.49287
2		0.48561		0.48907
3	0^h UT	0.48762	0^h UT	0.48906
4		0.48934		0.49075
5		0.49145		0.49206
6		0.49457		0.49352
0		0.38657		0.41941
1	02.2.61	0.38650	03.2.61	0.42298
2		0.38685		0.42098
3	15^h UT	0.38940	0^h UT	0.41670
4	(min)	0.39265		0.41369
5		0.39453		0.41367
6		0.39744		0.41484
0		0.50680		0.53816
1	08.2.61	0.50535	13.2.61	0.53699
2		0.50501		0.53594
3	0^h UT	0.50471	0^h UT	0.53596
4		0.50304		0.53542
5		0.50347		0.53496
6		0.50391		0.53485
0		0.58997		0.56344
1	18.2.61	0.58837	23.2.61	0.56292
2		0.58616		0.56218
3	0^h UT	0.58486	0^h UT	0.56242
4		0.58418		0.56275
5		0.58394		0.56354
6		0.58394		0.56501
0		0.51001		0.60811
1	28.2.61	0.50911	05.3.61	0.60656
2		0.50893		0.60440
3	0^h UT	0.50998	0^h UT	0.60288
4		0.51161		0.60163
5		0.51369		0.60077
6		0.51668		0.59964
0		0.60912		0.56937
1	05.3.61	0.60726	10.3.61	0.56781
2		0.60617		0.56551
3	9^h UT	0.60475	0^h UT	0.56502
4	(max)	0.60332		0.56438
5		0.60268		0.56433
6		0.60248		0.56438